The Anti-amyloid Compound DO1 Decreases Plaque Pathology and Neuroinflammation-Related Expression Changes in 5xFAD Transgenic Mice

Boeddrich, Annett ; Babila, Julius T ; Wiglenda, Thomas ; Diez, Lisa ; Jacob, Manuela ; Nietfeld, Wilfried ; Huska, Matthew R ; Haenig, Christian ; Groenke, Nicole ; Buntru, Alexander ; Blanc, Eric ; Meier, Jochen C ; Vannoni, Elisabetta ; Erck, Christian ; Friedrich, Beate ; Martens, Henrik ; Neuendorf, Nancy ; Schnoegl, Sigrid ; Wolfer, David P ; Loos, Maarten ; Beule, Dieter ; Andrade-Navarro, Miguel A ; Wanker, Erich E

Abstract: Self-propagating amyloid- (A) aggregates or seeds possibly drive pathogenesis of Alzheimer's disease (AD). Small molecules targeting such structures might act therapeutically in vivo. Here, a fluorescence polarization assay was established that enables the detection of compound effects on both seeded and spontaneous A 42 aggregation. In a focused screen of anti-amyloid compounds, we identified Disperse Orange 1 (DO1) ([4-((4-nitrophenyl)diazenyl)-N-phenylaniline]), a small molecule that potently delays both seeded and non-seeded A 42 polymerization at substoichiometric concentrations. Mechanistic studies revealed that DO1 disrupts preformed fibrillar assemblies of synthetic A 42 peptides and decreases the seeding activity of A aggregates from brain extracts of AD transgenic mice. DO1 also reduced the size and abundance of diffuse A plaques and decreased neuroinflammation-related gene expression changes in brains of 5xFAD transgenic mice. Finally, improved nesting behavior was observed upon treatment with the compound. Together, our evidence supports targeting of self-propagating A structures with small molecules as a valid therapeutic strategy.

DOI: https://doi.org/10.1016/j.chembiol.2018.10.013

The anti-amyloid compound DO1 decreases plaque pathology and neuroinflammation-related expression changes in 5xFAD transgenic mice

Annett Boeddrich[1#], Julius T. Babila[1#], Thomas Wiglenda[1#], Lisa Diez[1], Manuela Jacob[1], Wilfried Nietfeld[7], Matthew R. Huska[9], Christian Haenig[1], Nicole Groenke[1], Alexander Buntru[1], Eric Blanc[8], Jochen C. Meier[2], Elisabetta Vannoni[3], Christian Erck[4], Beate Friedrich[4], Henrik Martens[4], Nancy Neuendorf[1], Sigrid Schnoegl[1], David P. Wolfer[5], Maarten Loos[6], Dieter Beule[8], Miguel A. Andrade-Navarro[10], Erich E. Wanker[1*11]

1 Neuroproteomics, Max Delbrück Center for Molecular Medicine, 13125 Berlin, Germany
2 Division Cell Physiology, Technical University Braunschweig, 38106 Braunschweig, Germany
3 Children‘s Hospital Zurich - Eleonore Foundation, University of Zurich, 8032 Zurich, Switzerland
4 Synaptic Systems GmbH, 37079 Göttingen, Germany
5 Institute of Anatomy, University of Zurich and Institute of Human Movement Sciences and Sport, ETH Zurich, 8092 Zurich, Switzerland
6 Sylics (Synaptologics B.V.), 1008 Amsterdam, Netherlands
7 Genome Regulation, Max Planck Institut for Molecular Genetics, 14195 Berlin, Germany
8 Core Unit Bioinformatics – CUBI, Berlin Institute of Health, 10117 Berlin, Germany
9 Evolutionary and cancer genomics, Max Delbrück Center for Molecular Medicine, 13125 Berlin, Germany
10 Institute of Molecular Biology, Computational Biology and Data Mining, Johannes Gutenberg University, 55122 Mainz, Germany
11 Lead Contact

# Authors contributed equally

* To whom correspondence should be addressed: ewanker@mdc-berlin.de

Summary

Self-propagating amyloid-β (Aβ) aggregates or seeds possibly drive pathogenesis of Alzheimer's disease (AD). Small molecules targeting such structures might act therapeutically *in vivo*. Here, a fluorescence polarization (FP) assay was established that enables the detection of compound effects on both seeded and spontaneous Aβ42 aggregation. In a focused screen of anti-amyloid compounds, we identified DO1 [4-((4-nitrophenyl)diazenyl)-*N*-phenylaniline], a small molecule that potently delays both seeded and non-seeded Aβ42 polymerization at substoichiometric concentrations. Mechanistic studies revealed that DO1 disrupts preformed fibrillar assemblies of synthetic Aβ42 peptides and decreases the seeding activity of Aβ aggregates from brain extracts of AD transgenic mice. DO1 also reduced the size and abundance of diffuse Aβ plaques and decreased neuroinflammation-related gene expression changes in brains of 5xFAD transgenic mice. Finally, improved nesting behavior was observed upon treatment with the compound. Together, our evidence supports targeting of self-propagating Aβ structures with small molecules as a valid therapeutic strategy.

Introduction

Alzheimer's disease (AD) is a late onset progressive disorder characterized by memory loss and severe personality changes (Masters et al., 2015). In 2015, an estimated 23-33 million patients suffered from this most common form of dementia worldwide. Numbers are likely to double, if not treble, by 2050 (Winblad et al., 2016), unless effective, disease-modifying therapies that halt or delay progression become available.

The deposition of amyloid-β (Aβ) peptides in large, insoluble extracellular amyloid plaques is a pathological hallmark of AD (Masters et al., 2015; Selkoe and Hardy, 2016). Studies over the past decades, however, have suggested that small, soluble Aβ aggregates might also be relevant for neuronal toxicity and disease (Benilova et al., 2012). Such highly dynamic structures, detectable with biochemical methods and conformation-specific antibodies in brains of patients and AD transgenic mice, have been demonstrated to cause dysfunction and toxicity in various cellular models (Walsh et al., 2002). Recently, experimental evidence was provided that structural variants of fibrillar Aβ aggregates prepared from patient brains correlate with specific clinical subtypes (Qiang et al., 2017). In transgenic mice, these aggregates act as templates that can convert Aβ peptides from a soluble to an aggregated state (Jucker and Walker, 2013). This phenomenon, often termed "seeding" or "self-propagation", was studied *in vivo,* in brains of AD transgenic mice (Meyer-Luehmann et al., 2006) and *in vitro*, using protein misfolding cyclic amplification (PMCA) assays (Salvadores et al., 2014). Experimental evidence suggests that fibrillar Aβ aggregates with seeding activity might be a promising therapeutic target for AD. Small molecules that directly bind to such structures and

inhibit their seeding activity might have high potential to reduce symptoms in model organisms and patients.

A variety of small molecules have been described to directly target amyloidogenic Aβ peptides and interfere with their spontaneous self-assembly into β-sheet-rich, fibrillar aggregates (Hard and Lendel, 2012). This includes organic dyes like Congo red (Mathis et al., 2004) but also natural compounds such as (-)-epigallocatechin gallate (EGCG) or curcumin (Ehrnhoefer et al., 2008; Ono et al., 2004). The polyphenol EGCG, e.g., was shown to efficiently inhibit spontaneous Aβ fibrillization by directly binding to the unfolded polypeptides and promoting their conversion into off-pathway oligomers (Ehrnhoefer et al., 2008).

For most anti-amyloid compounds, however, mechanisms of action and exact molecular targets remain unclear (Young et al., 2017). It is unknown how they engage with aggregation-prone Aβ structures or whether they affect the activity of seeding-competent Aβ aggregates formed in brains of model organisms and patients. Previous investigations indicate that seed-mediated Aβ polymerization is more rapid than spontaneous aggregation (Harper and Lansbury, 1997), suggesting that inhibition of Aβ seeding with chemical compounds is more challenging. As a therapeutic strategy, however, it might be more promising, because seeding is a narrowly defined step in amyloidogenesis. Inhibiting it might halt progression of aggregate formation and disease. We hypothesize that only a fraction of the previously described amyloid targeting compounds might be active in seed-mediated Aβ polymerization reactions *in vitro*.

In this study, we first developed a fluorescence polarization (FP)-based assay in order to identify chemical compounds that influence Aβ42 polymerization under seeded and non-seeded conditions. Systematic compound testing with a small

focused library of potential amyloid-binding structures revealed the small molecule DO1 [4-((4-nitrophenyl)diazenyl)-*N*-phenylaniline], which most potently delayed both seeded and non-seeded Aβ42 aggregation in FP assays. For the screening, preformed fibrillar Aβ42 aggregates prepared from synthetic peptides were utilized to seed Aβ42 polymerization. Compound effects were also found with Aβ structures isolated from brains of AD transgenic mice, demonstrating that DO1 targets aggregates that are relevant to disease. Mechanistic studies in cell-free assays further substantiated the inhibitory effect of DO1 on seeded Aβ42 polymerization, indicating that the compound can disrupt preformed seeding-competent fibrillar structures. The potency of DO1 was finally investigated in 5xFAD transgenic mice, demonstrating a decrease of Aβ aggregates in brains and an improvement of nesting behavior. Strikingly, DO1 treatment also caused a decrease of abnormal inflammation-related expression changes in brains of these mice. The implications of our results for therapeutic strategies for AD and other amyloid diseases are discussed.

Results

Small molecules influence seed-mediated Aβ42 polymerization in FP assays

In previous studies chemical inhibitors of amyloid polymerization have been identified using Thioflavin T (ThT)-based aggregation assays (Arosio et al., 2014). ThT is a small benzothiazole molecule that changes its emission wavelength upon binding to fibrillar β-sheet-rich structures, enabling its application as a reporter molecule for quantifying the time-dependent formation of Aβ42 fibrils (Arosio et al., 2014). However, chemical compounds with emission wavelengths that overlap with that of aggregate-bound ThT cannot be investigated with ThT assays (Jameson et al., 2012). Also, a decrease in ThT fluorescence assumed to arise from inhibiting fibrillogenesis may simply be the result of compound binding to the ThT binding site on amyloid aggregates (Aitken et al., 2003). To overcome these limitations of the state-of-the-art ThT assay, we established a fluorescence polarization (FP)-based aggregation assay. The principle of this method is shown in **Figures 1A** and **1B**. In this assay, FP is used to study the time-dependent molecular interactions of Aβ42 peptides by monitoring the changes in the apparent size of interacting fluorescently labeled molecules over time. Aβ42 aggregation is reflected by an increase in the FP signal, which is proportional to a decrease in motility of fluorescently labeled Aβ42 assemblies as they grow larger through polymerization.

In proof-of-principle experiments, we first compared whether ThT- and FP-based amyloid polymerization assays yield similar kinetic profiles. We incubated Aβ42 monomers (10 µM) in the presence of ^{FAM}Aβ42 (0.05 µM) tracer in 384-well plates and quantified the increase of FP over time. Similarly, Aβ42 peptides (10 µM) were incubated in the presence of ThT (5 µM) in 384-well plates; fluorescence was measured at 440/485 nm. A concentration of 5 µM ThT was necessary to obtain a

reproducible signal-to-noise ratio. We found that FP- and ThT-based assays result in very similar Aβ42 aggregation profiles (**Figure S1A**), indicating that they both mirror the time-dependent formation of β-sheet-rich fibrillar structures from unstructured Aβ42 monomers.

Next, we assessed whether the established FP-based aggregation assay can be applied to quantify the seeding activity of preformed β-sheet-rich Aβ42 fibrils. We incubated 5-FAM-labeled (0.1 μM) and unlabeled (10 μM) Aβ42 monomers in the presence and absence of preformed Aβ42 fibrils (seeds) and monitored ^{FAM}Aβ42/Aβ42 co-polymerization by quantification of FP. We found that in the absence of seeds peptides spontaneously co-assemble into high-molecular-weight aggregates after a lag phase of ~6 h (**Figure 1C,** blue curve). Through the addition of Aβ42 seeds, however, the lag phase was shortened, indicating that seeding activity of synthetic Aβ42 assemblies can be quantified in a concentration-dependent manner. Biochemical studies confirmed that the preformed Aβ42 seeds added to FP reactions are ThT-reactive, β-sheet-rich fibrillar structures (**Figures S1B** and **S1C**).

We utilized the established FP assay to investigate the effects of selected small molecules on seed-mediated and spontaneous ^{FAM}Aβ42/Aβ42 co-polymerization. We selected 9 chemical compounds based on the following criteria: (1) they are already known to target amyloidogenic, aggregation-prone polypeptides or should be related to such structures (Jiang et al., 2013); (2) they should be small (< 500 Da) and lipophilic (Lipinski et al., 2001) in order to be orally active and to cross the blood-brain barrier (BBB) in mice (**Table S1**, compounds **#1 - #9**). Compounds were added at substoichiometric concentrations (1 μM) to FP reactions (10 μM Aβ42 and 0.1 μM ^{FAM}Aβ42 tracer) to avoid compound self-aggregation (Feng et al., 2008). Under these conditions, only **#4** (*N*,*N*-dimethyl-4-(phenyldiazenyl)aniline) efficiently

delayed both seeded and non-seeded Aβ42 polymerization in FP assays (**Figure S2A**).

To identify compounds that might be more potent than **#4**, we next tested 6 structurally related compounds in FP assays (**Table S1**, compounds **#10 - #15**). Seed-mediated ^{FAM}Aβ42/Aβ42 co-polymerization was most strongly delayed by compound **#15** [4-((4-nitrophenyl)diazenyl)-*N*-phenylaniline] (**Figure 1D**), which is related to compound **#4**. Interestingly, **#15** was significantly more effective than the closely related **#14**, which lacks the NO_2 group (**Figures 1D** and **S2B-S2D**), indicating that structure-activity relationships are detectable with FP assays. The effect of compound **#15** on seed-mediated Aβ42 polymerization was observed at different substoichiometric concentrations with an EC_{50} value of ~540 nM (**Figures 1E** and **1F**). Because of its high potency in FP assays, we focused on **#15** for all further experiments. Compound **#15** is an azo dye named Disperse Orange 1 (DO1) (David G. Whitten, 1971), which previously has not been described in the context of AD.

DO1 directly targets and disassembles preformed fibrillar Aβ42 aggregates

To investigate whether DO1 directly targets seeding-competent Aβ42 aggregates, we incubated a mixture of preformed fibrillar, β-sheet-rich Aβ42 aggregates for 24 h in the presence and absence of DO1 and subsequently separated soluble from insoluble structures by centrifugation. Then, supernatant and pellet fractions were analyzed with dot blot assays (DBAs) using the monoclonal anti-Aβ antibody 352, which specifically recognizes fibrillar assembles in DBAs (**Figures S3A** and **S3B**). This antibody was raised against preformed fibrillar Aβ42 aggregates

because the previously reported anti-fibril antibody OC (Kayed et al., 2007) revealed immunoreactivity for both Aβ42 monomers and aggregates (**Figure S3A**).

Analysis of untreated samples revealed 352-antibody immunoreactivity predominantly in the pellet fraction, indicating that larger protofibrillar and fibrillar Aβ42 aggregates are separated from smaller structures by centrifugation (**Figure 2A**). In DO1-treated samples, however, the immunoreactivity in pellet fractions was significantly decreased, while it was increased in the supernatant fractions (**Figures 2A** and **2B**), indicating that the compound converts larger Aβ42 assemblies into smaller structures. These results were also validated, when supernatant and pellet fractions from compound-treated and untreated samples were analyzed with DBAs using the monoclonal anti-Aβ antibodies 6E10 and 4G8 (**Figures 2A, S3C** and **S3D**), which preferentially recognize Aβ42 aggregates in DBAs (**Figure S3B**).

Next, we applied a native filter retardation assay (FRA) to investigate the size of preformed fibrillar Aβ42 aggregates in compound-treated and untreated samples. With this method, large protein assemblies can be separated from smaller ones through filtration (Wanker et al., 1999). Analysis of compound-treated and untreated samples revealed that DO1 treatment significantly decreases the immunoreactivity of Aβ42 species retained on cellulose acetate filter membranes, when supernatant and pellet fractions were analyzed (**Figures 2C** and **2D**), supporting the results with DBAs.

Finally, we analyzed the effect of DO1 on preformed, fibrillar Aβ42 aggregates by dynamic light scattering (DLS). With this technique, size distribution profiles of particles in suspension can be obtained without their separation on gels or membranes. DLS studies revealed that the size of Aβ42 aggregates in DO1-treated

samples was decreased in comparison to untreated samples (**Figure 2E**), confirming the results obtained with DBAs and native FRAs (**Figures 2A-2D**).

The NO_2 group in DO1 is critical for dissociation of fibrillar Aβ42 aggregates

To investigate whether the NO_2 group in DO1 is necessary for the disruption of fibrillar Aβ42 aggregates (**Figure 2A-2D**), we incubated preformed assemblies with DO1 or the related compound **#14,** lacking the NO_2 group (**Figure 1D**), for 24 h at 37 °C. Then, supernatant and pellet fractions were produced by centrifugation and analyzed with blue native gels and immunoblotting (**Figure 2F**). We detected both low-molecular-weight (LMWAs, ~60-200 kDa) and high-molecular-weight Aβ42 assemblies (HMWA, material retained in the gel pockets) in the supernatant fractions of untreated samples, while in the pellet fractions exclusively HMWAs were observed. In DO1 treated samples, however, the abundance of HMWAs in the pellet fractions was decreased in comparison to untreated controls, while the abundance of LMWAs in the supernatant fractions was increased (**Figure 2F**). This confirms our initial observations that DO1 disrupts preformed fibrillar Aβ42 aggregates and promotes the formation of smaller structures. Strikingly, such an effect was not observed when the samples were incubated with the related compound **#14** that lacks the NO_2 group (**Figures 1D** and **2F**).

DO1 treatment kinetically traps small, non-toxic Aβ42 oligomers

Our studies indicate that substoichiometric concentrations of DO1 can slow down Aβ42 fibrillogenesis (**Figures 1E** and **S2B**), suggesting that compound treatment may increase the abundance of small, proteotoxic Aβ42 oligomers in aggregation reactions. To address this question, we incubated monomers (0.05 μM ^{FAM}Aβ42 and 10 μM Aβ42) in the absence and presence of DO1 (1 and 5 μM) for 16 h at 37 °C. Then, samples were systematically analyzed by AFM. We observed a higher number of small spherical Aβ42 oligomers with a height of ~1 nm in DO1

treated than in untreated samples (**Figure 3A** and **3B**), indicating that the compound kinetically traps small prefibrillar Aβ42 structures. This was also confirmed when seeded compound-treated and untreated ^{FAM}Aβ42/Aβ42 co-polymerization reactions were analyzed (**Figures S4A** and **S4B**) or when spontaneous reactions were investigated by blue native PAGE and immunoblotting. In comparison to untreated samples, we observed an increase of LMWAs with a size of ~200-500 kDa in DO1-treated samples (**Figure 3C**), supporting the results obtained by AFM (**Figures 3A** and **3B**).

Finally, we carried out 3-(4,5-dimethylthiazol-2-yl)-2,5-diphenyltetrazolium bromide (MTT) reduction assays (Berridge et al., 2005) with PC12 cells to assess the toxicity of DO1 treated and untreated ^{FAM}Aβ42/Aβ42 co-aggregation reactions. In agreement with previous studies (Ehrnhoefer et al., 2008), formation of β-sheet-rich fibrillar aggregates (untreated samples) caused a pronounced inhibition of MTT reduction (~40%), indicative of cellular toxicity. However, inhibition of MTT reduction was significantly decreased with DO1 treated samples (**Figure 3D**), indicating that the compound-stabilized structures observed by AFM (**Figure 3A**) are less toxic than Aβ42 fibrils in cell-based assays.

DO1 decreases seeding activity of Aβ aggregates prepared from AD mouse brains

Previous studies suggest that seeding-competent Aβ aggregates in brains of AD patients and transgenic mice are responsible for disease progression and development (Jucker and Walker, 2013). We therefore addressed the question of whether DO1 can influence the seeding activity of potentially disease-relevant Aβ aggregates prepared from brains of AD transgenic mice (Heilbronner et al., 2013).

To prepare such structures, brain extracts from 22-month-old APPPS1 mice were first immunoprecipitated with beads using the monoclonal anti-Aβ antibodies 6E10 and 352 (**Figure 3E**). The precipitated material was then released from the beads by sonication and analyzed by SDS-PAGE and immunoblotting. We found that both anti-Aβ antibodies precipitated high molecular weight Aβ aggregates (retained in the gel pockets) from mouse brain extracts (**Figure 3E**). In contrast, such structures were not enriched from brain extracts with the control antibody IgG1.

Next, the prepared fractions were treated with DO1 and added as "seeds" to FP-based aggregation assays. We observed a pronounced shortening of the lag phase when 352 or 6E10 immunoprecipitates were added to FP assays (**Figures 3F** and **S4C**). In contrast, no such an effect was obtained with IgG1 immunoprecipitates (control), indicating that only antibody-enriched Aβ aggregates possess seeding activity. Finally, we found that DO1 treatment in a concentration-dependent manner extends the lag phase of Aβ aggregation in FP assays (**Figures 3F** and **S4C**), indicating that the compound directly targets disease-relevant Aβ structures and reduces their seeding activity.

DO1 decreases the formation of Aβ aggregates in brains of 5xFAD mice

Based on our seeding studies with Aβ aggregates from mouse brains (**Figure 3F**), we hypothesized that DO1 might also show activity *in vivo*. To address this question, we first assessed whether DO1 enters the brain. The compound was administered orally and the concentration was measured in crude brain extracts after acetonitrile precipitation by RP-LC-MS. We readily detected DO1 in mouse brain homogenates (**Figure S5A**), indicating that the compound crosses the blood-brain barrier. Next, we performed a histopathological examination of DO1-treated wild-type

mice to assess potential toxic effects of the chemical compound. We treated groups of mice by oral gavage with 2, 30 and 150 mg/kg DO1 once daily for 7 days. Mice were observed regularly; no overt toxic signs were detectable. After 7 days, mice were sacrificed and organs such as brain, heart, liver, lung, stomach, intestine, spleen and kidney were evaluated histopathologically. No macroscopic and microscopic changes related to DO1 treatment were detected, indicating that mice can be treated with this compound without major adverse effects.

We administered DO1 orally for 8 months to 6 week-old 5xFAD (Oakley et al., 2006) mice to study its effects on Aβ aggregation *in vivo*. Previous investigations indicate that the first amyloid plaques are detectable in brains of 5xFAD mice after ~2 months and increase in their abundance over time (Oakley et al., 2006). We administered the compound via compound-fortified food pellets (0.625 g/kg feed) and analyzed the impact of DO1 on Aβ aggregation in hippocampal brain regions at 9.5 months of age using immunohistochemical methods. For the detection of amyloid structures, the anti-Aβ antibodies 352 and 6E10 were applied. We observed that the numbers and sizes of antibody-reactive Aβ plaques were significantly decreased in compound-treated animals in comparison to untreated animals ($p < 0.001$; **Figures 4A-4C**). Interestingly, no significant compound effect was detected when Aβ plaques were stained with the dye Congo red (CR) (**Figure 4D**), which predominantly detects dense core regions in fibrillar Aβ plaques (Frid et al., 2007). This indicates that DO1 treatment diminishes the growth of the more diffuse outer spheres of Aβ plaques, which contain small fibrillar Aβ oligomers (Koffie et al., 2009), while it cannot alter the size of the congophilic dense core regions in amyloid plaques. A very similar result was obtained when cortical brain regions of DO1 treated and non-treated AD transgenic mice were analyzed (**Figures S5B-S5E**).

To further explore the effect of DO1 on plaque formation, we performed co-staining experiments with the dye Thioflavin S (ThS) and the antibody 352. Similar to CR, ThS predominantly detects dense core regions in amyloid plaques (McLellan et al., 2003). In comparison, the 352 antibody preferentially detected small fibrillar Aβ aggregates in DBAs (**Figure S3B**), suggesting that it might stain the outer spheres of amyloid plaques, which contain Aβ oligomers (Koffie et al., 2009). We found that the sizes of 352-reactive Aβ plaques were significantly decreased in compound-treated animals in comparison to untreated ones (**Figures 4E** and **4F**). In contrast, no significant compound effect was observed when ThS-positive dense core plaque regions were analyzed (**Figure 4G**).

Next, we assessed the abundance of Aβ aggregates in compound-treated and untreated AD mouse brains with a native FRA (Wanker et al., 1999) using the anti-Aβ antibody 352. We observed a significant decrease of 352-reactive Aβ aggregates in compound-treated samples compared to untreated controls (**Figures S5F** and **S5G**), supporting our results obtained with immunohistological methods (**Figures 4A** and **S5B**).

Finally, we investigated whether DO1 treatment alters the abundance of the marker protein GFAP (glial fibrillary acidic protein) in AD brains. Previous studies indicate that the formation of Aβ plaques in 5xFAD brains is associated with an increase of GFAP (Oakley et al., 2006), suggesting that a decrease in Aβ aggregates in DO1 treated mice might be accompanied by a decrease of this disease marker protein. Analysis of mouse brain extracts with ELISAs revealed significantly lower GFAP levels in DO1-treated AD animals than in untreated controls (**Figure S5H**), indicating that compound treatment (**Figures 4A-4C**) decreases the abundance of relevant marker proteins in AD brains.

DO1 treatment improves nesting behaviour in 5xFAD transgenic mice

To elucidate whether DO1 treatment influences behavioural deficits in AD transgenic mice, we assessed the ability of compound-treated and untreated animals to build nests, a natural social behaviour of mice requiring spatial memory and hippocampal neuronal functions that are affected in AD (Lin et al., 2007; Mufson et al., 2015). We treated 6 week-old female 5xFAD and wild-type control mice for 8 months with DO1 and subsequently assessed their nest-building ability using a standardized protocol (Deacon, 2006). At an age of 9.5 months, the AD transgenic mice exhibited a significant impairment in nesting behaviour compared to age-matched wild-type controls (**Figure 5A**). This behaviour, however, was significantly improved in DO1-treated AD transgenic mice. In order to validate the DO1 effect on nesting behaviour, we repeated the drug trial with 5xFAD transgenic mice in an independent research laboratory, this time using male mice to assess efficacy. In this validation study, 6-week-old male 5xFAD and control mice were treated with DO1 for 6 months. We found that DO1 treatment again significantly improved the nest building performance of AD transgenic mice (**Figure 5B**), essentially confirming the results from the initial drug trial with female mice.

DO1 reduces transcriptional changes related to neuroinflammation in brains of 5xFAD mice

Previous investigations indicate that the time-dependent deposition of Aβ aggregates in brains of 5xFAD transgenic mice correlates with global changes in gene expression (Landel et al., 2014). This includes increased expression of multiple transcripts encoding proteins involved in inflammation (Landel et al., 2014), suggesting that DO1 treatment might influence these expression changes in AD

brains. To test this hypothesis, we analyzed gene expression in brains of DO1 treated and untreated 5xFAD and control mice using a microarray technology (data accessible at NCBI GEO database (Edgar et al., 2002), accession GSE119756). DO1 was administered orally for 8 months to 6-week-old mice. In total, transcripts of 4 groups of treated and untreated mice (TG+DO1, TG, WT+DO1 and WT) were systematically investigated.

Principal component analysis (PCA) of the gene expression data showed that the samples clustered into four broad groups correlating with disease and treatment status. PCA revealed a clear separation of data obtained from AD and non-AD brains (**Figure 6A**), confirming previous observations (Landel et al., 2014). Furthermore, we observed that the compound DO1 alters the transcriptional profiles in brains of 5xFAD and wild-type control mice (**Figure 6A**).

We first compared the gene expression in brains of untreated 5xFAD and control mice. We found that 290 genes are differentially expressed in AD and non-disease (TGvsWT) brains, of which 257 genes (88.6%) were upregulated in AD brains, while 33 (11.4%) were downregulated (**Figure 6B**). We next investigated whether DO1 treatment influences the dysregulation in gene transcription in brains of 5xFAD transgenic mice. We observed 208 genes differentially expressed between DO1-treated AD and DO1-treated wild-type (WT) control (TG*vsWT*) animals, of which 204 (98.1%) and 4 (1.9%) genes were up- and downregulated, respectively (**Figure 6B**). This indicates that compound treatment decreases the number of significantly dysregulated genes in AD brains. In comparison, a higher number of differentially expressed genes was obtained when the data of DO1-treated AD and untreated WT control animals (TG*vsWT) were compared. In this case, 625 significantly dysregulated genes were obtained, of which 355 (56.8%) and 270 (43.2%) were up- and down-regulated, respectively. This supports the results of PCA

(**Figure 6A**), indicating that compound treatment leads to expression changes in both transgenic and WT brains. To assess the impact of DO1 on brains of WT control mice, we finally compared the gene expression data of compound-treated and untreated WT mice (WT*vsWT). In this case, we detected 203 significant expression changes (**Figure 6B**); 130 genes (64%) were up-regulated, 73 genes (36%) were down-regulated, confirming our assumption that chronic DO1 treatment induces transcriptional changes in WT mouse brains.

We used ingenuity pathway analysis (IPA, Kramer et al., 2014), to identify the pathways that are potentially altered in brains of DO1-treated and untreated transgenic and WT mice. Analysis of TGvsWT, TG*vsWT* and TG*vsWT datasets revealed gene expression changes predominantly in neuroinflammation signaling pathways (**Figures S6A-S6C**), confirming previous reports (Landel et al., 2014). The analysis of the WT*vsWT dataset, however, revealed significant expression changes in the cholesterol biosynthesis pathway (**Figure S6D**), suggesting that DO1 alters pathways in WT brains that are distinct from TG animals. Previous investigations revealed that in 5xFAD mice many well-known markers of microglia cells and astrocytes such as TREM-2 (triggering receptor expressed on myeloid cells 2) or GFAP are upregulated in comparison to WT controls (Landel et al., 2014). We therefore inspected the top 20 upregulated genes in the TGvsWT dataset for genes that are typically activated in AD brains. We found a large number of well-known inflammation and immune markers such as Cst7 (Cystatin F) or TREM-2 (**Figure 6C**). Furthermore, an upregulation of the astrocyte marker GFAP was observed, confirming our results obtained with ELISAs (**Figure S5H**). Together these results support our hypothesis that the deposition of Aβ aggregates leads to activation of microglia and astrocytes in brains of 5xFAD mice.

We finally assessed whether compound treatment leads to quantitative changes in the transcript levels of genes that are upregulated both in the TGvsWT and TG*vsWT* datasets. We identified 186 shared genes in these datasets (**Figure 6D**). Importantly, we found that DO1 treatment significantly counteracts upregulation of genes in 5xFAD brains (**Figure 6E**). The results are shown for the 20 top upregulated genes in **Figure 6C**. Very similar results were obtained when the expression of upregulated genes in the TG*vsWT dataset was analyzed (**Figures 6F-6H**).

Discussion

Here, we describe a drug discovery strategy to identify small molecules that decrease the seeding activity of fibrillar, β-sheet-rich Aβ structures *in vitro* and *in vivo*. This strategy involves: (1) the identification of compounds that reduce the seeding activity of preformed, fibrillar Aβ42 aggregates with a FP-based amyloid polymerization assay, (2) the investigation of compound effects on preformed Aβ42 seeds with biochemical and biophysical methods, (3) the analysis of compound effects on potentially disease-relevant Aβ seeds prepared from brains of AD transgenic mice and (4) the investigation of selected compounds in the progressive, well-described 5xFAD transgenic AD mouse model (Oakley et al., 2006). In a proof-of-concept study, we identified the aromatic small molecule DO1 [4-((4-nitrophenyl)diazenyl)-*N*-phenylaniline] that potently decreases the activity of synthetic and mouse-derived Aβ seeds in cell-free FP assays (**Figures 1E** and **1F**). Also, it is active *in vivo* in the brains of transgenic 5xFAD mice. This model bears five mutations linked to familial forms of AD and recapitulates the main features of the disease in a few months (Oakley et al., 2006). Treatment with DO1 not only decreased fibrillar Aβ aggregates (**Figures 4A** and **4E**) but also neuroinflammatory gene expression changes (**Figures 6E-6H**) associated with amyloid deposition and improved a behavioural phenotype, i.e. nesting (**Figures 5A** and **5B**).

In contrast to previously reported Aβ aggregation modulators such as tramiprosate (Gervais et al., 2007), RS-0406 (Nakagami et al., 2002), RO90-7501 (Bohrmann et al., 2000) or scyllo-inositol (McLaurin et al., 2002), DO1 can decrease the seeding activity of preformed Aβ42 fibrils at substoichiometric concentrations in FP assays (**Figure S2**). This suggests that the molecular mechanism by which DO1 perturbs Aβ42 aggregation is distinct from previously described small molecules. We

hypothesize that DO1 directly targets and disrupts seeding-competent, fibrillar Aβ42 structures in aggregation reactions and that this specific activity is responsible for the observed extension of the lag phase and the delay of Aβ42 fibril growth (**Figure 1E**). It is important to note that both fibrillar and pre-fibrillar aggregates are formed during the lag phase in Aβ42 polymerization reactions (Lee et al., 2011); both may be targeted by DO1. More detailed investigations using biochemical, structural and biophysical methods are necessary to elucidate the precise mechanism of action of DO1 in seeded and non-seeded Aβ42 polymerization reactions. These studies should also involve the focused analysis of the impact of the compound on primary and secondary nucleation as well as on fibril elongation, as all these three microscopic processes are operative during the lag phase in Aβ42 amyloid aggregation (Arosio et al., 2015).

DO1 treatment significantly decreases the size and the abundance of Aβ plaques in brains of 5xFAD transgenic mice (**Figures 4A-C**). Focused histological studies revealed that especially the diffuse outer spheres of amyloid plaques were significantly reduced, while the dense core regions were not influenced (**Figures 4D** and **4G**). Previous studies indicate that synaptic transmission is severely impaired in brains of 5xFAD mice and that this deficiency correlates with the high abundance of diffuse amyloid plaques (Crouzin et al., 2013), suggesting that these structures contribute to the development of AD-related symptoms. Small, fibrillar Aβ oligomers were shown to be enriched in the outer spheres of amyloid plaques (Koffie et al., 2009). We hypothesize that DO1 decreases the abundance of diffuse amyloid plaques because it directly targets self-propagating, fibrillar Aβ aggregates and promotes their dissociation and degradation. This activity may also be responsible for the compound's effect on immune hyperactivity, caused by Aβ plaque-associated

microglia (Landel et al., 2014). Thus, we suggest a similar mechanism of action of DO1 both *in vitro* and *in vivo*.

Our studies indicate that the Aβ aggregate-targeting compound DO1 has beneficial effects on the disease process in 5xFAD transgenic mice. This is in agreement with previously reported observations: Inhibiting seed-mediated Aβ aggregation with the FDA-approved drugs mitoxantrone and bithonol reduced synapse loss and neuronal damage in APP transgenic mice (Eleuteri et al., 2015). Similarly, cognitive deficits were decreased when transgenic APP/PS1 mice were treated with the small molecule EPPS, which can disaggregate higher-molecular-weight Aβ structures in cell-free assays (Kim et al., 2015). Thus, our observations with DO1 are not without precedent and provide compelling support for the amyloid hypothesis.

Significance

Several small molecules targeting the aggregation process of the Aβ peptide have been reported. How they act at the molecular level and whether they influence seed-mediated Aβ polymerization, a process which happens faster than spontaneous Aβ aggregation and has recently emerged as the potential driver of disease, is largely unknown. We have developed an FP-based Aβ polymerization assay and could show that it identifies potent modulators of both seeded and spontaneous Aβ aggregation. Using it, we have discovered a compound, DO1, that targets preformed Aβ aggregates and efficiently reduces their seeding activity at substoichiometric concentrations. DO1 is also active *in vivo*. It improves plaque pathology and behaviour and reduces immune hyperactivity of Aβ plaque-associated microglia in transgenic Alzheimer mice. Our evidence supports the hypothesis that seeding-

competent, fibrillar amyloid aggregates are disease-relevant structures (Tipping et al., 2015) and that targeting them with small molecules is a promising therapeutic strategy. We regard DO1 as a tool compound investigated in a proof-of-concept study. We intend to stimulate further research and development to find improved, structurally related molecules that bring about a therapeutic effect by targeting seeding-competent amyloid aggregates and their propagation. We do not wish to suggest in any way that DO1 can already be used for medication. On the contrary, comprehensive pharmacological and toxicological assessment, i.e. hit-to-lead development, would be required prior to a potential evaluation in a clinical trial.

Acknowledgements

We thank D. Kleckers, S. Neuendorf, G. Grelle, S. Rautenberg, L. Brusendorf, A. Sabah and K. Bach for technical assistance. We would like to thank Dr. Zoltán Cseresnyés (Confocal and 2-Photon Microscopy Core Facility, MDC, now HKI Jena) for his technical assistance concerning mouse brain imaging and Prof. Frank Heppner (Department of Neuropathology, Charité University Medicine Berlin) for providing APPPS1 AD mouse brain tissues. For performing mouse experiments, we thank R. van der Loo, B. Koopmans and R. Wijnands from Sylics**,** Amsterdam. We thank C. Meyer, I. Drescher and A. Rhyner from the University of Zurich for evaluation of mouse behavior and Prof. Dr. Hans-Peter Lipp (University of Zurich) for expert discussions. This study received funding from the GO-Bio Initiative of the German Federal Ministry for Education and Research (BMBF), grant no. 0313881, the ERA-NET NEURON initiative, funded by the BMBF, grant no. 01W1301, the Berlin Institute of Health Collaborative Research Grant no. 1.1.2.a.3 funded by the BMBF, the Helmholtz Validation Fund grant no. HVF-0013 funded by the Helmholtz Association, Germany, (to E.E.W.), and the Max Delbrück Center for Molecular Medicine in the Helmholtz Association for application-oriented research (to A. Boe. and E.E.W.). In addition, this work was supported by grants from the BMBF (Era-Net NEURON II CIPRESS to J.C.M.), the Helmholtz Association (VH-NG-246 to J.C.M.), and the Deutsche Forschungsgemeinschaft DFG (Priority Programme SPP 1784 ME2075/7-1 to J.C.M.); the European Union FP7 (HEALTH-F2-2009-241498) EUROSPIN to M.L./Sylics, H.M./Synaptic Systems, D.P.W. and E.E.W.

Author contributions

A.B., B.J.T., T.W., M.J, L.D., N.G., J.C.M., A.B. and N.N. planned and performed compound screening, biochemical analysis, mouse and analytical experiments; E.V. and D.P.W. planned and performed mouse behavior experiments; C.E., B.F. and H.M. generated the antibody 352 from antigenic material provided by the MDC; M.L. realized a mouse compound trial; C.H., M.H., E.B, D.B., M.A.A-N performed gene expression analysis; W.N. performed RNA amplification, labeling, and hybridization experiments; S.S., A.B, B.J.T., T.W., C.H. and E.E.W coordinated the study and edited the manuscript; E.E.W designed the study and wrote the manuscript.

Declaration of Interests

The authors declare no competing interests.

References

Aitken, J.F., Loomes, K.M., Konarkowska, B., and Cooper, G.J. (2003). Suppression by polycyclic compounds of the conversion of human amylin into insoluble amyloid. The Biochemical journal *374*, 779-784.

Arosio, P., Knowles, T.P., and Linse, S. (2015). On the lag phase in amyloid fibril formation. Phys Chem Chem Phys *17*, 7606-7618.

Arosio, P., Vendruscolo, M., Dobson, C.M., and Knowles, T.P. (2014). Chemical kinetics for drug discovery to combat protein aggregation diseases. Trends in pharmacological sciences *35*, 127-135.

Arras, M., Autenried, P., Rettich, A., Spaeni, D., and Rulicke, T. (2001). Optimization of intraperitoneal injection anesthesia in mice: drugs, dosages, adverse effects, and anesthesia depth. Comparative medicine *51*, 443-456.

Assenov, Y., Ramirez, F., Schelhorn, S.E., Lengauer, T., and Albrecht, M. (2008). Computing topological parameters of biological networks. Bioinformatics *24*, 282-284.

Benilova, I., Karran, E., and De Strooper, B. (2012). The toxic Abeta oligomer and Alzheimer's disease: an emperor in need of clothes. Nat Neurosci *15*, 349-357.

Berridge, M.V., Herst, P.M., and Tan, A.S. (2005). Tetrazolium dyes as tools in cell biology: new insights into their cellular reduction. Biotechnology annual review *11*, 127-152.

Bohrmann, B., Adrian, M., Dubochet, J., Kuner, P., Muller, F., Huber, W., Nordstedt, C., and Dobeli, H. (2000). Self-assembly of beta-amyloid 42 is retarded by small molecular ligands at the stage of structural intermediates. Journal of structural biology *130*, 232-246.

Crouzin, N., Baranger, K., Cavalier, M., Marchalant, Y., Cohen-Solal, C., Roman, F.S., Khrestchatisky, M., Rivera, S., Feron, F., and Vignes, M. (2013). Area-specific alterations of synaptic plasticity in the 5XFAD mouse model of Alzheimer's disease: dissociation between somatosensory cortex and hippocampus. PLoS One *8*, e74667.

David G. Whitten, P.D.W., J. G. Pacifici, and Gether Irick Jr. (1971). Solvent and substituent on the thermal isomerization of substituted azobenzenes. Flash spectroscopic study. Journal of the American Chemical Society *93*.

Deacon, R.M. (2006). Assessing nest building in mice. Nat Protoc *1*, 1117-1119.

Dunning, M.J., Smith, M.L., Ritchie, M.E., and Tavare, S. (2007). beadarray: R classes and methods for Illumina bead-based data. Bioinformatics *23*, 2183-2184.

Edgar, R., Domrachev, M., and Lash, A.E. (2002). Gene Expression Omnibus: NCBI gene expression and hybridization array data repository. Nucleic acids research *30*, 207-210.

Ehrnhoefer, D.E., Bieschke, J., Boeddrich, A., Herbst, M., Masino, L., Lurz, R., Engemann, S., Pastore, A., and Wanker, E.E. (2008). EGCG redirects amyloidogenic polypeptides into unstructured, off-pathway oligomers. Nature structural & molecular biology *15*, 558-566.

Eleuteri, S., Di Giovanni, S., Rockenstein, E., Mante, M., Adame, A., Trejo, M., Wrasidlo, W., Wu, F., Fraering, P.C., Masliah, E.*, et al.* (2015). Novel therapeutic strategy for neurodegeneration by blocking Abeta seeding mediated aggregation in models of Alzheimer's disease. Neurobiol Dis *74*, 144-157.

Feng, B.Y., Toyama, B.H., Wille, H., Colby, D.W., Collins, S.R., May, B.C., Prusiner, S.B., Weissman, J., and Shoichet, B.K. (2008). Small-molecule aggregates inhibit amyloid polymerization. Nat Chem Biol *4*, 197-199.

Frid, P., Anisimov, S.V., and Popovic, N. (2007). Congo red and protein aggregation in neurodegenerative diseases. Brain research reviews *53*, 135-160.

Gervais, F., Paquette, J., Morissette, C., Krzywkowski, P., Yu, M., Azzi, M., Lacombe, D., Kong, X., Aman, A., Laurin, J.*, et al.* (2007). Targeting soluble Abeta peptide with Tramiprosate for the treatment of brain amyloidosis. Neurobiol Aging *28*, 537-547.

Geumann, C., Gronborg, M., Hellwig, M., Martens, H., and Jahn, R. (2010). A sandwich enzyme-linked immunosorbent assay for the quantification of insoluble membrane and scaffold proteins. Analytical biochemistry *402*, 161-169.

Hard, T., and Lendel, C. (2012). Inhibition of amyloid formation. J Mol Biol *421*, 441-465.

Harper, J.D., and Lansbury, P.T., Jr. (1997). Models of amyloid seeding in Alzheimer's disease and scrapie: mechanistic truths and physiological consequences of the time-dependent solubility of amyloid proteins. Annu Rev Biochem *66*, 385-407.

Heilbronner, G., Eisele, Y.S., Langer, F., Kaeser, S.A., Novotny, R., Nagarathinam, A., Aslund, A., Hammarstrom, P., Nilsson, K.P., and Jucker, M. (2013). Seeded strain-like transmission of beta-amyloid morphotypes in APP transgenic mice. EMBO Rep *14*, 1017-1022.

Hothorn T, H.K., A, v.d.W.M., H, W., and A, Z. (2017). Package 'coin', Conditional Inference Procedures in a Permutation Test Framework. R Foundation for Statistical Computing.

Jameson, L.P., Smith, N.W., and Dzyuba, S.V. (2012). Dye-binding assays for evaluation of the effects of small molecule inhibitors on amyloid (abeta) self-assembly. ACS chemical neuroscience *3*, 807-819.

Jiang, L., Liu, C., Leibly, D., Landau, M., Zhao, M., Hughes, M.P., and Eisenberg, D.S. (2013). Structure-based discovery of fiber-binding compounds that reduce the cytotoxicity of amyloid beta. eLife *2*, e00857.

Jucker, M., and Walker, L.C. (2013). Self-propagation of pathogenic protein aggregates in neurodegenerative diseases. Nature *501*, 45-51.

Kauffmann, A., Gentleman, R., and Huber, W. (2009). arrayQualityMetrics--a bioconductor package for quality assessment of microarray data. Bioinformatics *25*, 415-416.

Kayed, R., Head, E., Sarsoza, F., Saing, T., Cotman, C.W., Necula, M., Margol, L., Wu, J., Breydo, L., Thompson, J.L.*, et al.* (2007). Fibril specific, conformation dependent antibodies recognize a generic epitope common to amyloid fibrils and fibrillar oligomers that is absent in prefibrillar oligomers. Molecular neurodegeneration *2*, 18.

Kim, H.Y., Kim, H.V., Jo, S., Lee, C.J., Choi, S.Y., Kim, D.J., and Kim, Y. (2015). EPPS rescues hippocampus-dependent cognitive deficits in APP/PS1 mice by disaggregation of amyloid-beta oligomers and plaques. Nat Commun *6*, 8997.

Koffie, R.M., Meyer-Luehmann, M., Hashimoto, T., Adams, K.W., Mielke, M.L., Garcia-Alloza, M., Micheva, K.D., Smith, S.J., Kim, M.L., Lee, V.M.*, et al.* (2009). Oligomeric amyloid beta associates with postsynaptic densities and correlates with excitatory synapse loss near

senile plaques. Proceedings of the National Academy of Sciences of the United States of America *106*, 4012-4017.

Kramer, A., Green, J., Pollard, J., Jr., and Tugendreich, S. (2014). Causal analysis approaches in Ingenuity Pathway Analysis. Bioinformatics *30*, 523-530.

Landel, V., Baranger, K., Virard, I., Loriod, B., Khrestchatisky, M., Rivera, S., Benech, P., and Feron, F. (2014). Temporal gene profiling of the 5XFAD transgenic mouse model highlights the importance of microglial activation in Alzheimer's disease. Molecular neurodegeneration *9*, 33.

Lee, J., Culyba, E.K., Powers, E.T., and Kelly, J.W. (2011). Amyloid-beta forms fibrils by nucleated conformational conversion of oligomers. Nat Chem Biol *7*, 602-609.

LeVine, H., 3rd (1999). Quantification of beta-sheet amyloid fibril structures with thioflavin T. Methods Enzymol *309*, 274-284.

Lin, L., Chen, G., Kuang, H., Wang, D., and Tsien, J.Z. (2007). Neural encoding of the concept of nest in the mouse brain. Proceedings of the National Academy of Sciences of the United States of America *104*, 6066-6071.

Lipinski, C.A., Lombardo, F., Dominy, B.W., and Feeney, P.J. (2001). Experimental and computational approaches to estimate solubility and permeability in drug discovery and development settings. Advanced drug delivery reviews *46*, 3-26.

Masters, C.L., Bateman, R., Blennow, K., Rowe, C.C., Sperling, R.A., and Cummings, J.L. (2015). Alzheimer's disease. Nat Rev Dis Primers *1*, 15056.

Mathis, C.A., Wang, Y., and Klunk, W.E. (2004). Imaging beta-amyloid plaques and neurofibrillary tangles in the aging human brain. Curr Pharm Des *10*, 1469-1492.

McLaurin, J., Golomb, R., Jurewicz, A., Antel, J.P., and Fraser, P.E. (2000). Inositol stereoisomers stabilize an oligomeric aggregate of Alzheimer amyloid beta peptide and inhibit abeta -induced toxicity. J Biol Chem *275*, 18495-18502.

McLellan, M.E., Kajdasz, S.T., Hyman, B.T., and Bacskai, B.J. (2003). In vivo imaging of reactive oxygen species specifically associated with thioflavine S-positive amyloid plaques by multiphoton microscopy. J Neurosci *23*, 2212-2217.

Meyer-Luehmann, M., Coomaraswamy, J., Bolmont, T., Kaeser, S., Schaefer, C., Kilger, E., Neuenschwander, A., Abramowski, D., Frey, P., Jaton, A.L.*, et al.* (2006). Exogenous induction of cerebral beta-amyloidogenesis is governed by agent and host. Science *313*, 1781-1784.

Mufson, E.J., Mahady, L., Waters, D., Counts, S.E., Perez, S.E., DeKosky, S.T., Ginsberg, S.D., Ikonomovic, M.D., Scheff, S.W., and Binder, L.I. (2015). Hippocampal plasticity during the progression of Alzheimer's disease. Neuroscience *309*, 51-67.

Nakagami, Y., Nishimura, S., Murasugi, T., Kaneko, I., Meguro, M., Marumoto, S., Kogen, H., Koyama, K., and Oda, T. (2002). A novel beta-sheet breaker, RS-0406, reverses amyloid beta-induced cytotoxicity and impairment of long-term potentiation in vitro. Br J Pharmacol *137*, 676-682.

Oakley, H., Cole, S.L., Logan, S., Maus, E., Shao, P., Craft, J., Guillozet-Bongaarts, A., Ohno, M., Disterhoft, J., Van Eldik, L.*, et al.* (2006). Intraneuronal beta-amyloid aggregates,

neurodegeneration, and neuron loss in transgenic mice with five familial Alzheimer's disease mutations: potential factors in amyloid plaque formation. J Neurosci *26*, 10129-10140.

Ono, K., Hasegawa, K., Naiki, H., and Yamada, M. (2004). Curcumin has potent anti-amyloidogenic effects for Alzheimer's beta-amyloid fibrils in vitro. J Neurosci Res *75*, 742-750.

Paxinos, G., and Franklin, K.B.J. (2008). The Mouse Brain in Stereotaxic Coordinates. Academic Press, New York, USA.

Qiang, W., Yau, W.M., Lu, J.X., Collinge, J., and Tycko, R. (2017). Structural variation in amyloid-beta fibrils from Alzheimer's disease clinical subtypes. Nature *541*, 217-221.

R_Core_Team (2006). R: A language and environment for statistical computing. R Foundation for Statistical Computing.

Ritchie, M.E., Phipson, B., Wu, D., Hu, Y., Law, C.W., Shi, W., and Smyth, G.K. (2015). limma powers differential expression analyses for RNA-sequencing and microarray studies. Nucleic acids research *43*, e47.

Salvadores, N., Shahnawaz, M., Scarpini, E., Tagliavini, F., and Soto, C. (2014). Detection of misfolded Abeta oligomers for sensitive biochemical diagnosis of Alzheimer's disease. Cell Rep *7*, 261-268.

Sedgewick, J. (2008). Scientific Imaging with Photoshop: Methods, Measurement, and Output. New Riders, Pearson Education, USA, 98.

Selkoe, D.J., and Hardy, J. (2016). The amyloid hypothesis of Alzheimer's disease at 25 years. EMBO Mol Med *8*, 595-608.

Tipping, K.W., van Oosten-Hawle, P., Hewitt, E.W., and Radford, S.E. (2015). Amyloid Fibres: Inert End-Stage Aggregates or Key Players in Disease? Trends Biochem Sci *40*, 719-727.

Walsh, D.M., Klyubin, I., Fadeeva, J.V., Cullen, W.K., Anwyl, R., Wolfe, M.S., Rowan, M.J., and Selkoe, D.J. (2002). Naturally secreted oligomers of amyloid beta protein potently inhibit hippocampal long-term potentiation in vivo. Nature *416*, 535-539.

Wanker, E.E., Scherzinger, E., Heiser, V., Sittler, A., Eickhoff, H., and Lehrach, H. (1999). Membrane filter assay for detection of amyloid-like polyglutamine-containing protein aggregates. Methods Enzymol *309*, 375-386.

Wilcock, D.M., Gordon, M.N., and Morgan, D. (2006). Quantification of cerebral amyloid angiopathy and parenchymal amyloid plaques with Congo red histochemical stain. Nature protocols *1*, 1591-1595.

Winblad, B., Amouyel, P., Andrieu, S., Ballard, C., Brayne, C., Brodaty, H., Cedazo-Minguez, A., Dubois, B., Edvardsson, D., Feldman, H.*, et al.* (2016). Defeating Alzheimer's disease and other dementias: a priority for European science and society. Lancet Neurol *15*, 455-532.

Young, L.M., Ashcroft, A.E., and Radford, S.E. (2017). Small molecule probes of protein aggregation. Curr Opin Chem Biol *39*, 90-99.

Figure legends

Figure 1 (see also Figures S1 and S2). Establishment of a fluorescence polarization-based Aβ42 aggregation assay.

(**A**) Assay principle. Fluorescently labeled Aβ42 peptides (tracer) are incorporated into growing Aβ42 aggregates during the aggregation process. 1) Initially, reactions are dominated by small structures, rotating rapidly in solution. 2) As polymerization proceeds, larger aggregates rotating more slowly are formed.

(**B**) Time-dependent reduction of tracer mobility in the course of aggregation results in an increase of the polarization signal (milli-polarization, mP). 1) Highly mobile, non-incorporated tracer molecules emit light in various planes of oscillation. 2) Incorporated tracer molecules emit fluorescent light predominantly in the excitation plane.

(**C**) Concentration-dependent seeding effect of preformed fibrillar aggregates (FAs; 5 to 200 nM monomer equivalent) in FP assays. Average values were derived from quadruplicates of each sample.

(**D**) Structural formula of compounds #14 and #15/ DO1.

(**E**) Concentration-dependent effect of DO1 (0.05 to 2.5 µM) on seed-mediated ^{FAM}Aβ42 (0.1 µM)/Aβ42 (10 µM) co-aggregation in FP assays. Average values were derived from triplicates of each sample.

(**F**) Calculation of the EC_{50} value for DO1 from aggregation profiles shown in ***E*** at 5.5 h.

Data in ***C***, ***E*** and ***F*** are represented as mean ± SD.

Figure 2 (see also Figure S3). Effects of DO1 on fibrillar Aβ42 assemblies.

(**A**) Dot-blot assays (DBAs) of DO1-treated and untreated (control, ctrl) Aβ42 fibrillar aggregates (FAs). After DO1 treatment (24 h, 37 °C) Aβ42 FAs were centrifuged; supernatant (S) and pellet (P) fractions were analyzed by DBAs using the antibodies 352, 4G8 and 6E10. Quadruplicates per sample were analyzed. A representative experiment is shown.

(**B**) Box plot of relative quantification of 352 antibody immunoreactivity shown in ***A***. Two-way analysis of ANOVA showed a significant DO1 treatment effect ($F_{2,18}$ = 63.32, p = 7.16e-09) and position (antibody reactivity in pellet versus supernatant) effect ($F_{1,18}$ = 13.20, p = 0.0019). There was also a significant interaction between treatment and position effects ($F_{2,18}$ = 152.86, p = 5.08e-12), indicating that DO1 converts larger fibrillar Aβ42 aggregates into smaller structures.

(**C**) Analysis of supernatant and pellet fractions as in ***A*** by filter retardation assay (FRA). Prior to the preparation of supernatant and pellet fractions, preformed Aβ42 FAs (equivalent to a monomer concentration of 1 µM) were incubated with a 5-fold molar excess of DO1 for 24 h at 37 °C. Aβ42 species retained on filter membranes were detected with 6E10.

(**D**) Box plot quantification of triplicate samples from native FRAs shown in ***C***. Treatment with DO1 significantly decreased the 6E10 immunoreactivity both in the supernatant (p = 9.892e-06) and the pellet (p = 4.823e-05) fractions. p-values were calculated with unpaired two tailed t-test.

(**E**) Analysis of DO1-treated and untreated pellet fractions by dynamic light scattering (DLS). The size distribution of Aβ42 aggregate species is shown.

(**F**) Analysis of supernatant (S) and pellet (P) fractions of DO1- or #14-treated samples by native PAGE and Western blotting. For immunoblotting, the anti-Aβ antibody 4G8 was used.

Figure 3 (see also Figure S4). DO1 traps small Aβ42 oligomers and reduces the seeding activity of Aβ aggregates prepared from AD mouse brains.

(**A**) AFM analysis of aggregate species derived from compound treated and untreated ^{FAM}Aβ42 (0.05 µM)/Aβ42 (10 µM) co-aggregation reactions after incubation for 18 h. Samples were analyzed using the AFM probe PPP-NCHAuD. Color gradient: 0-10 nm height.

(**B**) Number of oligomers were counted in three different areas (0.5 x 0.5 µm each) of respective AFM pictures in ***A***. *** $p<0.001$, * $p<0.05$, one-way ANOVA. Data show mean ± SEM.

(**C**) Analysis of ^{FAM}Aβ42/Aβ42 co-assemblies shown in ***A*** after 18 h by native PAGE and immunoblotting using the anti-Aβ antibody 6E10.

(**D**) MTT assay. Effects of DO1 treated and untreated Aβ42 aggregation reactions after 18 h (shown in ***A***) on MTT reduction in PC12 cells. As a control, cells were treated with 0.05 µM and 0.25 µM DO1 alone, which is equivalent to the amount of compound added to cells in ^{FAM}Aβ42/Aβ42 aggregation reactions. Values represent percentage of buffer control. Statistical significance was assessed by one-way ANOVA followed by Dunnett's multiple comparison post hoc test. **, $p\leq0.01$.

(**E**) Analysis of immunoprecipitates prepared from APPPS1 mouse brain extracts by SDS-PAGE and immunoblotting. IP: immunoprecipitation; Aβ-specific antibodies: 352 and 6E10; control antibody: IgG1. Precipitated Aβ aggregates are indicated with asterisks. Input: 10% brain homogenate; FT, flow-through; Wash: wash fractions. Immunoblot: 6E10 antibody; HC, heavy chain; LC, light chain.

(**F**) Effects of different concentrations of DO1 on seeding activity of Aβ species immunoprecipitated from APPPS1 mouse brain homogenates (6E10-IP). Average values derived from quadruplicates of each sample in the experiment.

Data in ***D*** and ***F*** are represented as mean ± SD.

Figure 4 (see also Figure S5). Effects of DO1 on amyloid-β plaques in 5xFAD transgenic mice.

(**A**) Immunohistochemical detection of Aβ plaques in the hippocampus of 5xFAD female mice treated for 8 months with 0.652 g DO1 per kg of mouse chow. Top and middle rows, 3,3'-diaminobenzidine (DAB) staining of Aβ plaques with 352 and 6E10 antibodies. Bottom row, Congo red staining of Aβ plaques. Scale bar is equal to 50 μm and applies to all images.

(**B-C**) Quantification of 352 (**B**) and 6E10 (**C**) immunoreactivities; ***$p < 0.001$ versus control, one-way ANOVA, n = 4-5 mice per group.

(**D**) Quantification of Congo red stained dense core plaques in hippocampal regions.

(**E**) Analysis of hippocampal brain sections of female DO1-treated and untreated 5xFAD transgenic mice by immunofluorescence microscopy. Top, 352-reactive regions. Middle, Thioflavin S (ThS) staining of dense core regions. Bottom, 3-dimensional merge of ThS and 352 antibody stains. The scale bar is equal to 200 μm.

(**F-G**) Quantification of 352- (**F**) and ThS-stained (**G**) Aβ plaques in mouse brains (***$p < 0.001$, one-way ANOVA, n = 4 mice per group).

Data in ***B - D***, ***F*** and ***G*** are represented as mean ± SEM.

Figure 5 (see also Figure S5). Effects of DO1 on nesting behavior of 5xFAD transgenic mice.

(A) Nest building activity of 9.5 month-old female wild-type (Wt) and 5xFAD transgenic (Tg) mice treated with DO1. DO1-treated transgenic mice were compared to untreated transgenic control mice (genotype Chi-Square = 25.797, df = 3, p-value = 1.052e-5, Kruskal-Wallis Test; p-value = 0.0003013 [treated versus control 5xFAD], pairwise exact Wilcoxon Test, n = 14-19).

(**B**) Nest building activity of male wild-type (Wt) and 5xFAD transgenic (Tg) mice treated with DO1. The compound significantly improved the nestlet quality score of 7.5 month-old male AD mice in an independent experiment (Chi-squared = 8.9374, df = 3, p-value = 0.03013, Kruskal-Wallis Test; p-value = 0.01204 [treated versus control 5xFAD], pairwise exact Wilcoxon Test, n = 15 -18).

Figure 6 (see also Figure S6). Differential gene expression analysis of DO1 treated and untreated 5xFAD and control mice.

(**A**) Principal component analysis of untreated and DO1 treated wildtype (WT, WT*) and transgenic mice (TG, TG*) based on log2 normalized gene expression values.

(**B**) Overview of significantly ($p < 0.05$) up- (red) and down-regulated (blue) genes in untreated und treated groups of WT and TG mice. The statistical significance was assessed with an unpaired, two-tailed t-test (***$p < 0.0001$).

(**C**) Top 20 up-regulated genes from TGvsWT and TG*vsWT* gene expression datasets.

(**D**) Intersection of upregulated genes in TGvsWT and TG*vsWT* gene expression datasets.

(**E**) Comparison of the log2 (fold change) of the intersection of upregulated genes in TGvsWT and TG*vsWT* datasets. Boxplots extend from the lower to the upper

quartiles, with the internal lines referring to the median values. Statistical significance was assessed by a paired, two-tailed t-test (***p < 0.0001).

(**F**) Top 20 up-regulated genes from TGvsWT and TG*vsWT gene expression datasets.

(**G**) Intersection of upregulated genes in TGvsWT and TG*vsWT datasets.

(**H**) Comparison of the log2 (fold change) of the intersection of upregulated genes in TGvsWT and TG*vsWT datasets. Boxplots extend from the lower to the upper quartiles, with the internal lines referring to the median values. Statistical significance was assessed by a paired, two-tailed t-test (***p < 0.0001).

STAR METHODS

Key Resources Table

Contact for Reagent and Resource Sharing

Experimental Model and Subject Details

Mouse models and breeding

Nest building

Brain tissue processing

Method Details

Aβ42 peptide preparation

Fluorescence polarization-based aggregation assay

Antibodies

Small molecules

Light scattering

Dot blot assay

Native filter retardation assay

Denaturing filter retardation assay

Native gels

Centrifugation experiments with Aβ42 FAs

Thioflavin T assay

Atomic Force Microscopy (AFM)

Homogenization of mouse brain tissues

Immunoprecipitation of Aβ aggregates

Western blot analysis

MTT assay

Detection of DO1 in mouse brain tissues

Quantification of GFAP with ELISA

Immunohistochemistry and Congo red staining

Assessment of amyloid load

Extraction of mRNAs and quality analysis

RNA amplification, labeling, and hybridization

Differential gene expression analysis

Principal component analysis (PCA)

IPA pathway analysis

Quantification and Statistical Analysis

Statistical analysis

Data and Software Availability

Contact for Reagent and Resource Sharing

Further information and requests for resources and reagents should be directed to and will be fulfilled by the lead contact, E. E. Wanker (ewanker@mdc-berlin.de).

Experimental Models and Subject Details

Mouse models and breeding. Hemizygous male 5xFAD mice [B6SJL-Tg(APPSwFlLon,PSEN1*M146L*L286V 6799Vas/jax] (Oakley et al., 2006) on a 50:50 C57BL/6J x SJL/J (BL6SJL) background were mated to female BL6SJLF1/J mice. Resulting offspring were weaned at approximately three weeks of age; genotyping for the APP transgene and the blind mutation was performed by PCR with tissue biopsies (Oakley et al., 2006). 5xFAD transgenic mice overexpress two human AD-related proteins: the mutant human APP (695) protein with the Swedish (K670N), Florida (I716V) and the London (V717I) mutations and the human PS1 protein with the mutations M146L and L286V. Treatment of mice with DO1 started at an age of six weeks. Animal care was in accordance with the Directive 2010/63/EU of

the European Parliament and the Council on the protection of animals used for scientific purposes. All experimental procedures were approved by the local animal welfare authority in Berlin, Germany under license number TVV G0077/07. Mice were group-housed (5/cage) with wood shavings. Environmental enrichment was achieved by providing each cage with a play tunnel, shredded paper and a wood block. Food and water were provided *ad libitum*. All mice in the DO1 group received DO1-supplemented pelleted mouse chow at a concentration of 0.652 g/kg food.

Nest building. Approximately one hour before the dark phase (light-dark phase 12 h:12 h), each mouse was given 3 g of nestlet made of pressed cotton (Lillico, Surrey, UK). The nests were assessed the next morning as described before (Deacon, 2006). The scoring scale for nestlet usage was: 1, >90% intact; 2, 50-90% intact; 3, 10-50% intact; 4, 0-10% intact, flat nest; 5, 0-10% intact, crater-shaped nest. In another evaluation, the untorn nesting material was weighed after brushing off loose material and bedding wood chips and subtracted from the initial weight to obtain nestlet usage in percent.

Brain tissue processing. Animals were transcardially perfused with 25 ml 0.9% saline under deep anesthesia using ketamin (65 mg/kg), xylazin (13 mg/kg) and acepromazin (2 mg/kg) (Arras et al., 2001). Mice were sacrificed by cervical dislocation; brains were removed and divided into hemispheres. The left hemisphere was used for biochemistry while the right hemisphere was used for immunohistochemistry. The right hemisphere was post-fixed by immersion in 4% PFA (pH 7.2-7.4) overnight. The brains were cryoprotected by transferring them into a solution of 30% sucrose in phosphate buffer, pH 7.4 supplemented with 0.1% sodium azide and stored at 4 °C for 48 hours. Following cryoprotection, the brains

were frozen in isopentane and stored at -80 °C until use. Hemibrains were sectioned coronally (+2.25 mm to -3.5 mm bregma) using a cryostat (Leica Biosystems, Eisfeld, Germany). 25 µm thick sections were collected (approximately 27 sections per brain) and stored in cryoprotectant antifreeze solution (30% ethylene glycol and 30% glycerol in 0.2 M phosphate buffer, pH 7.2) at -20 °C for further processing.

Method Details

Aβ42 peptide preparation. Synthetic amyloid-β (1-42) peptide (Aβ42) produced by the laboratory of Dr. Volkmar-Engert (Institute for Medical Immunology, Charité, Berlin, Germany) was dissolved in 1,1,1,3,3,3-Hexafluoro-2-propanol (HFIP) at a concentration of 5 mg/ml. The solution was vortexed and incubated for 4 h at 20 °C. Every hour, samples were sonicated for 10 min in a sonicator bath. Incubation of the Aβ42 peptide in HFIP was continued for 16 h at 20 °C. Finally, sonicated material (30 min) was aliquoted and lyophilized. Monomeric Aβ42 solutions for Thioflavin T (ThT) binding assays were prepared by dissolving the lyophilized HFIP-treated peptide at a concentration of 200 µM in 10 mM NaOH, followed by 1 min vortexing and 5 min sonication in a sonicator bath. For preparation of fibrillar Aβ42 aggregates (FAs) lyophilized HFIP-treated Aβ42 peptide was thawed on ice and dissolved at a concentration of 10 mg/ml in 100 mM NaOH. After 1 min vortexing and 5 min sonication in a sonicator bath, low salt buffer (LSB: 1.9 mM KH_2PO_4, 8.1 mM K_2HPO_4, 10 mM NaCl, pH 7.4) was added yielding an Aβ42 concentration of 200 µM. After 6 h incubation at 37 °C with 300 rpm shaking, the Aβ42 solution was aliquoted and stored at -80 °C until use. The morphology and stability of FAs was analyzed by atomic force microscopy, native gels, dot blots and ThT binding assays. For fluorescence polarization (FP) assays, Aβ42 peptide was purchased from Bachem

(Bubendorf, Switzerland, #H-1368). Peptide was dissolved in 1,1,1,3,3,3-Hexafluoro-2-propanol (HFIP) to a concentration of 5 mg/ml, vortexed for 1 min and sonicated for 10 min at 4 °C in a sonicator bath. Then, the solution was incubated for 3 h at 22 °C, with 1 min vortexing and 1 min sonication every hour. After incubation for further 67 h at 22 °C, samples were aliquoted and lyophilized (RVC 2-25 CDplus, Christ, Osterode am Harz, Germany). Monomeric Aβ42 solutions were prepared from lyophilized peptide aliquots by dissolving them in 10 mM NaOH to yield a final Aβ42 concentration of 200 µM followed by 1 min vortexing and 5 min sonication. To start aggregation reactions for FP assays 200 µM monomeric Aβ42 peptide was diluted in LSB to yield a concentration of 10 µM.

Fluorescence polarization-based aggregation assay.

5-Carboxyfluorescein labeled β-amyloid (1-42) peptide (5-FAM; Anaspec, Fremont, CA, USA) was dissolved in 1 mM NaOH to 50 µM and stored as a stock solution at -20 °C. 0.1 µM of this tracer together with 10 µM Aβ42 monomer in LSB were combined with 40 nM (monomer equivalent) Aβ42 FAs (seeds) and test compounds (1 µM). The aggregation mixtures were replenished with LSB to a total volume of 40 µl. The fluorescence polarization measurements were carried out every 15 min at 37 °C for a minimum of 12h in a plate-reader (Infinite M1000/ Infinite M1000 PRO, Tecan, Männedorf, Switzerland) at an excitation wavelength of 470 ± 5 nm and an emission wavelength of 528 ± 20 nm in 384-well plates with 5 sec shaking before each read. Values are means of five technical replicates. Polarization values are expressed as dimensionless milli-polarization (mP) values, calculated by the plate-reader software i-control (Tecan, Männedorf, Switzerland).

Antibodies. To generate a monoclonal antibody that preferentially recognizes Aβ42 FAs, the prepared amyloid species were injected into mice and hybridomas were generated by a proprietary immunization protocol of Synaptic Systems Göttingen (see also https://www.sysy.com/services/index.php). Three 8-10 week-old BALB/c female mice were subcutaneously immunized with Aβ42 FAs over a period of 17 days. Cells from the knee lymph nodes were fused with the mouse myeloma cell line P3X63Ag8.653 (ATCC CRL-1580). The clones used in this study were re-cloned two times by limiting dilution and the immunoglobulin subclass was determined.

Antibodies secreted by the hybridomas were screened for their reactivity against the immunogen using ELISA. Positive antibodies were retested with ELISA against Aβ42 FAs and monomers. Hybridomas producing antibodies with preference for Aβ42 FAs were subcloned to monoclonality and further analyzed by histology and Western blotting. One of the antibodies showing specificity for Aβ42 FAs was the antibody 352. Commercially available antibodies applied in this study are: anti-β-amyloid 1-16 antibody (clone 6E10, Biolegend, San Diego, CA, USA); anti-β-amyloid 17-24 antibody (clone 4G8, Biolegend, San Diego, CA, USA); anti-amyloid fibrils OC antibody (Merck Millipore, Darmstadt, Germany); anti-mouse IgG1 isotype control (ThermoFisher Scientific, Waltham, MA, USA); anti-mouse IgG, peroxidase conjugated for immunoblots (Sigma-Aldrich, Taufkirchen, Germany); mouse monoclonal GFAP antibody and rabbit polyclonal GFAP antibody (Synaptic Systems, Göttingen, Germany); goat anti-mouse IgG and peroxidase AffiniPure goat anti-rabbit IgG for ELISA (Jackson Immuno Research Laboratories, West Grove, PA, USA); Alexa Fluor 488 goat anti-mouse IgG (Invitrogen, Waltham, MA, USA); peroxidase conjugated goat anti-mouse IgG (Jackson Immuno Research Laboratories, West Grove, PA, USA).

Small molecules. Compounds for primary screens and hit validation were purchased from Arcos Organics (Belgium) at the purity specified by the supplier given in %: #9, 95%; #10, 99%; #12, 95%; #14, ≥97%; #15, ≥97%; Sigma-Aldrich (Taufkirchen, Germany): #3, ≥98%; #7, ≥98%; #8, 65-75%; Fluka (Taufkirchen, Germany): #4, ≥98%; #6 ≥97%; Aldrich (St. Louis, USA): #11, ≥95%; #13, 95%; Riedel-de-Haën (Seelze, Germany): #2, ≥97%. Compounds #1, ≥95% and #5, ≥95% were synthesized by Chiroblock GmbH (Bitterfeld-Wolfen, Germany). Compounds were dissolved in Dimethyl sulfoxide (DMSO) at 20 mM and stored at -20 °C.

Light scattering. Experiments were performed on a Zetasizer nano (Malvern Instruments Ltd., Malvern, UK) in a sealed quartz cuvette using a sample volume of 80 µl. Samples were sonicated for 10 sec in a water bath before measuring. Total scattering intensities were recorded over time from seven technical repetitions, each accumulating 30 single measurements.

Dot blot assay. For dot blot assays, Aβ42 solutions were spotted onto nitrocellulose membrane (Amersham Protran 0.1 µm NC, GE Healthcare Life Sciences, Munich, Germany). After washing the membrane with 1x PBS (13.7 mM NaCl, 0.27 mM KCl, 1 mM Na_2HPO_4, 0.2 mM KH_2PO_4, pH 7.4), it was blocked for 30 min with 3% skim milk (Sigma-Aldrich, Taufkirchen, Germany) in 1x PBS containing 0.05% Tween 20 (PBS-T). Then, the membrane was incubated over night with the primary antibody diluted in 3% skim milk PBS-T. Subsequently, the membrane was washed three times for 10 min in PBS-T and incubated with the secondary peroxidase-conjugated anti-mouse antibody for 1 h at room temperature. The membrane was washed two times for 5 min in PBS-T and two times for 10 min in PBS; immunoreactive protein

was detected using ChemiGlow (Biozym, Hess. Oldendorf, Germany). Chemiluminescence was measured with a FujiFilm LAS-3000 and images were quantified using the Aida image analysis software (Raytest, Straubenhardt, Germany).

Native filter retardation assay. Samples were filtered through a cellulose acetate membrane with a pore size of 0.2 µm (GE Healthcare Life Sciences, Munich, Germany). Then, the membrane was washed with 1x PBS and blocked for 30 min with 3% skim milk in PBS-T. The protein aggregates retained on filter membranes were finally detected by antibody-based reactions as described for the dot blot assays.

Denaturing filter retardation assay. Samples were incubated with 2% SDS and 50 mM DTT for 5 min at 95°C and then filtered through a 0.2 µm cellulose acetate membrane preequilibrated in 0.1% SDS. Following, the membrane was washed with 0.1% SDS and then used for immunodetection of aggregates as described for the dot blot assays.

Native gels. For analysis on native gels, Aβ42 solutions were mixed with NativePAGE 4x sample buffer and loaded onto a NativePAGE Novex 4-16% Bis-Tris gel (ThermoFisher Scientific, Waltham, MA; USA). As a molecular weight marker, the NativeMark unstained protein standard was used (ThermoFisher Scientific, Waltham, MA, USA). NativePAGE was performed according to a standard protocol. Then, proteins were transferred to a nitrocellulose membrane (0.45 µm; GE Healthcare Life Sciences, Munich, Germany) using a semi-dry Western blotting protocol. Proteins of

interest were detected on the membrane by an antibody-based reaction as described for the dot blot assays.

Centrifugation experiments with Aβ42 FAs. Preformed fibrillar Aβ42 aggregates (1 µM, calculated from the molecular weight of Aβ42 monomers) were incubated for 24 h with 1 µM (1x) or 5 µM (5x) compound solutions in low salt buffer (LSB) at 37 °C. As a control, the compound solvent was used. Then, the samples were centrifuged at 18,000 x g for 30 min at 4 °C. The supernatant was carefully removed and transferred to a new tube. The pellet was solubilized in LSB in a volume equivalent to the supernatant, vortexed and sonicated for 1 min in a sonicator bath. Lastly, supernatant and pellet fractions were analyzed with dot blots, filter retardation assays and native gels.

Thioflavin T assay. Aβ42 monomers and fibrillar aggregates (4.5 µM, monomer equivalent) were mixed with 20 µM Thioflavin T (ThT) in 1x PBS in a volume of 100 µl. Fluorescence measurements of samples were performed in a plate reader (Infinite M200, Tecan, Männedorf, Switzerland) at an excitation wavelength of 420 nm and an emission wavelength of 485 nm (LeVine, 1999). For kinetic measurements Aβ42 monomers (10 µM) were mixed in LSB buffer with ThT (5 µM). Thioflavin T (ThT) fluorescence intensity measurements were performed in quadruplicates in black non-binding 384-well microtiter plates (Greiner Bio-One) in a total volume of 40 µl. The measurements were carried out every 15 min for 20 hours at 37 °C. Prior to each measurement the samples were shaken for 5 seconds with an amplitude of 2 mm. Fluorescence measurements were performed in a plate reader (Infinite M1000 PRO; Tecan, Männedorf, Switzerland) using the following

wavelengths: Ex: 440 nm/Em: 485 nm.

Atomic Force Microscopy (AFM). For AFM analysis sheet mica (Glimmer V3; Plano, Wetzlar, Germany) were glued to a microscope slide and samples (10 µl of 2.5 µM FA or monomer solutions, 20 µl of ^{FAM}Aβ42 (0.05 µM)/Aβ42 (10 µM) co-aggregation reactions) were adsorbed for 10 min onto the freshly cleaved mica, washed with freshly filtered deionized water (4 × 20 µl) and dried overnight. Dry AFM images were recorded on a Nanowizard II/Zeiss Axiovert setup (JPK) using intermittent contact mode and FESP silicon (Bruker AFM Probes, Camarillo, CA; USA) or PPP-NCHAuD probes (NANOSENSORS™, Neuchâtel, Switzerland).

Homogenization of mouse brain tissues. Frozen tissue was weighed and homogenized in a 5-fold excess (w/v) of ice cold 50 mM Tris-HCl pH 7.5, 150 mM NaCl, 0.1% SDS, 0.5% Sodium deoxycholate, 1% Triton X-100, 0.25 U/µl Benzonase and a complete protease inhibitor cocktail using a Schütt Homogen Plus (Schütt-Biotec GmbH, Göttingen, Germany) semi-automatic homogenizer (700 rpm). The homogenate was centrifuged for 20 min at 1,500 x g at 4 °C to remove cell debris. The supernatant was then transferred to a new tube and the total protein concentration was determined with the Pierce BCA assay (ThermoFisher Scientific, Waltham, MA, USA) using BSA as a standard. The supernatant was analyzed by native filter retardation assays. Furthermore, seeding-competent Aβ aggregate species were enriched by immunoprecipitation from mouse brain homogenates.

Immunoprecipitation of Aβ aggregates. Seeding-competent Aβ aggregate species were enriched from mouse brain homogenates (prepared from 0.25 mg brain tissue

of APPPS1 transgenic mice) through immunoprecipitation with magnetic protein G beads (ThermoFisher Scientific, Waltham, MA, USA) coated with 6E10 or 352 antibody, respectively. Antibody bound beads were incubated with homogenate at room temperature for 30 min. Beads were then washed three times in LSB before sonification for 30 sec with a *Sonic Dismembrator Ultrasonic Processor* (ThermoFisher Scientific, Waltham, MA, USA, *FB-120,* 5/64" tip). Seeding-competent Aβ aggregate species (10 µl) released from beads by sonication were analyzed in FP assays.

Western blot analysis. Protein extracts or magnetic protein G beads with immunoprecipitated Aβ aggregate species were boiled with NuPAGE 4x sample buffer for 5 min and then loaded onto NuPAGE Novex 4-12% Bis-Tris gels (ThermoFisher Scientific, Waltham, MA, USA). Electrophoresis was performed according to a standard protocol followed by transfer of proteins onto a nitrocellulose membrane (0.45 µm; GE Healthcare Life Sciences, Munich, Germany) using a wet blotting system (BioRad, Munich, Germany). The generated blots were incubated with primary 6E10 (1:1000, Biolegend, San Diego, CA, USA) and HRP-conjugated secondary (1:2000, Sigma-Aldrich, Taufkirchen, Germany) antibodies. Immunoreactive proteins on membranes were visualized with WesternBright Quantum chemiluminescence substrate (Advansta, Menlo Park, CA, USA).

MTT assay. PC12 cells were plated at a density of 15,000 cells per well on clear 96-well plates in 90 µl fresh medium (RPMI 1640 (1x) medium supplemented with 10 % horse serum, 5 % FBS and 100 U/ml penicillin and streptomycin) in a 5 % (v/v) CO_2 humidified environment at 37°C. After 48 h, Aβ aggregate species were added (final concentration: 0.5 µM) and cells were further incubated for 1 day at 37°C.

Cytotoxicity was measured using an MTT assay kit (Promega). Absorbance values of formazan were determined at 570 nm using an Infinite spectrometer (Tecan). Statistical significance was assessed by one-way ANOVA followed by Dunnett's post hoc test. **, $p \leq 0.01$.

Detection of DO1 in mouse brain tissues. This study was performed at Pharmacelsus GmbH (Saarbruecken, Germany). In brief, for oral administration DO1 was freshly dissolved in an aqueous 1% methyl cellulose solution. After DO1 administration of 10 mg per kg mouse weight with an application volume of 10 ml/kg, mice were perfused with PBS and sacrificed by cervical dislocation at the indicated time points. Brains were removed, homogenized with 1 volume of PBS using a Precellys Dual homogenizer (Peqlab, Erlangen, Germany) with ceramic beads. A volume of 20 µl of the resulting homogenate was clarified by acetonitrile (ACN, 40 µl) precipitation. The resulting supernatant was analyzed by LC-MS using a phenyl-hexyl phase (Accucore, 2.1×50 mm ID, 2.6 µm, RP159, Thermo Fisher Scientific, Dreieich, Germany) for separation (mobile phase A: H_2O + 0.2% Heptafluorobutyric acid (HFBA), mobile phase B: ACN + 0.2% HFBA, % B (t (min)), 80(0-0.1)-3(0.4-1.7)-80(1.8-2.5)) and Q-Exactive mass spectrometer (Thermo Fisher Scientific, Dreieich, Germany) for detection (mode: H-ESI, positive ion). Diclofenac was used as internal standard; for calibration spiked blank brain tissue samples were used.

Quantification of GFAP with ELISA. For quantification of GFAP (glial fibrillary acidic protein) with ELISA, mouse brains were homogenized in 50 mM Tris-HCl pH 8 (300 mg/ml w/v) with a complete protease inhibitor cocktail and 0.25 U/µl Benzonase using the Schütt Homgen Plus semi-automatic homogenizer. After 10 min incubation of the homogenate at 4 °C, SDS was added to a final concentration of 1.2% and

incubation was continued for 15 min at room temperature. Then, the homogenate was diluted with five volumes of ice cold 1.2% Triton X-100 and centrifuged at 100,000 x g for 30 min to remove the insoluble material (Geumann et al., 2010). The supernatant was finally transferred to a new tube and protein concentration was determined using the Pierce™ BCA assay (ThermoFisher Scientific, Waltham, MA, USA). The protein BSA was utilized as a standard. The GFAP ELISA was performed according to standard protocols (Geumann et al., 2010). A mouse monoclonal GFAP antibody (concentration 500 ng/ml) and a rabbit polyclonal GFAP antibody (diluted 1:2000) were used as capture and detection antibodies, respectively. As a protein standard, different concentrations of recombinant full-length human GFAP protein (Synaptic Systems, Göttingen, Germany) were used.

Immunohistochemistry and Congo red staining. Congo red staining was performed as described (Wilcock et al., 2006) with slight modifications. Brain sections taken from cryoprotectant solution were washed three times for 5 min in PBS. The sections were mounted onto slides and air-dried for 20 min at room temperature. Slides were incubated in 0.02 M NaOH in 80% ethanol saturated with NaCl for 20 min followed by a 45 min incubation in 0.15% (w/v) Congo red (Sigma-Aldrich, Taufkirchen, Germany) in 0.02 M NaOH in 80% ethanol saturated with NaCl. Stained sections were rinsed eight times each in 95% ethanol and 100% ethanol, followed by three times for 5 min incubation in Roti©-Histoclear and mounting with Roti©-Histokitt (Carl Roth, Karlsruhe, Germany). Primary antibodies for immunohistochemistry were mouse monoclonal antibodies 6E10 against human Aβ at 1:1000 dilution and 352 against fibrillar Aβ oligomers at 1:1000 dilution. Secondary antibodies were: Alexa Fluor 488 goat anti-mouse IgG (Invitrogen, Waltham, MA, USA) at 1:2000 dilution;

peroxidase-conjugated goat anti-mouse IgG (Jackson Immuno Research Laboratories, West Grove, PA, USA) at 1:300 dilution.

Assessment of amyloid load. Sections stained for Congo red positive plaques or Aβ immunohistochemistry were scanned using a Nikon Super Coolscan 9000 film scanner (Nikon, Düsseldorf, Germany) with a gamma of 1 (Sedgewick, 2008) at 4000 dpi. Images were exported to ImageJ for color deconvolution using the plugin (http://www.dentistry.bham.ac.uk/landinig/software/cdeconv/cdeconv.html) to subtract cresyl counterstain color. The cortex and hippocampus were manually outlined with the Volocity software (Perkin Elmer, Rodgau-Jügesheim, Germany); number of pixels and total pixel areas occupied by both structures were determined. Monochromatic-based thresholding was used to quantify pixels occupied by Congo red-positive or immunolabeled plaques. The number of plaques and percentage of brain regions occupied by them were determined. Seven brain sections separated by 200 µm beginning from bregma -0.82 (Paxinos and Franklin, 2008) were evaluated for each mouse. The treatment status of the mice was unknown to the investigator during analysis.

Extraction of mRNAs and quality analysis. Freshly isolated mouse brains were dissected and cortex was isolated. RNA was prepared from mouse tissues using the „RNeasy Lipid Tissue Mini Kit“ (Qiagen, Hilden, Germany). DNA was removed from the RNA sample using the „RNase-Free DNase Set“ kit from Qiagen (Hilden, Germany). The quality and yield of extracted total RNAs were analyzed on Agilent RNA 6000 Nano Chips by the 2100 Bioanalyzer (Agilent Technologies, Waldbronn, Germany) and on the NanoDrop ND-1000 UV-Vis Spectrophotometer (Thermo Scientific, Darmstadt, Germany).

RNA amplification, labeling, and hybridization. 500 ng of total RNA in 11 µl RNase free water was used as starting material for the generation of biotin-labeled cRNA with the Illumina® TotalPrep™ RNA Amplification Kit (ThermoFisher Scientific, Dreieich, Germany), following supplier instructions. cRNA was cleaned up with cRNA filter cartridges before use for subsequent hybridization on Illumina® Sentrix BeadChips (Illumina, San Diego, USA). To perform whole genome expression analysis MouseWG-6 v2.0 Expression BeadChips, were incubated with biotin labeled cRNA for 18 h at 58°C in a hybridization oven under humidity-controlled conditions. After hybridization, the Illumina® Sentrix BeadChips were washed using buffers provided by the kit. 2.5 µl (1 mg/ml) of Streptavidin-Cy3 (per Chip) diluted in 2.5 ml blocking buffer were incubated per Chip for 10 minutes under gentle shaking conditions to allow binding of cRNA to gene-specific probes. After washing, Illumina® Sentrix BeadChips were dried and scanned using the Illumina BeadArray Reader GX (Illumina, San Diego, USA). To quantify gene expression signal levels we used the Illumina's BeadStudio software (Illumina, San Diego, USA) package.

Differential gene expression analysis. The analysis was carried out using the limma package in R. Probes were identified as differentially expressed for Benjamini and Hochberg adjusted p-value of < 0.05, and an absolute fold change $> 50\%$.

Principal component analysis (PCA). We first selected the probes that had a normalized value of expression above 6.5 (which is roughly the median value of expression in most samples) in at least 5 out of the 23 samples used in this study. This was done to make sure that low expression probes do not have too much of an impact on the PCA. This step removed 20811 of 46235 (approximately 45%) probes.

The resulting filtered dataset was then mean centered and scaled so that the values had a standard deviation of one. The PCA was performed with these values.

Ingenuity pathway analysis (IPA). The differentially expressed genes (DEGs, $p < 0.05$) from the sample comparisons TGvsWT, TG*vsWT*, TG*vsWT and WT*vsWT were used for pathway analysis. The 10 most significant canonical pathways were selected using the Ingenuity Pathway Analysis (IPA) software tool (https://www.qiagenbioinformatics.com/products/ingenuity-pathway-analysis/).

Quantification and Statistical Analysis

Statistical analysis. Statistical analysis was performed using the R programming environment (Assenov et al., 2008; Hothorn T et al., 2017; R_Core_Team, 2006), the scientific data analysis software GraphPad Prism version 7.04 for Windows, GraphPad Software, La Jolla, California, USA, www.graphpad.com and the Student's t-Test of the CSBSJU Minnesota (http://www.physics.csbsju.edu/stats/t-test.html). Individual statistical methods are indicated in the figure legends. Statistical significance is indicated in the text and figure legends as $*p < 0.05$, $**p < 0.01$ and $***p < 0.001$.

Data and Software Availability

The microarray dataset contains the expression values of 23 samples tested against 46,000 Illumina Probe IDs, of which 27,000 gave a positive signal. An MS Excel spreadsheet contains the values for these signals. The 23 samples are named using a combination of a barcode number and a letter that refers to one of the 4 groups of tissues from treated and untreated mice (TG+DO1, TG, WT+DO1 and WT), from which the samples were derived. The columns to the right of the signal values for the

23 samples show additional identifying information for the individual Illumina probes. The expression of 878 transcripts was changed significantly and used for further bioinformatics analyses. Another Excel spreadsheet provides detailed information for the 23 samples derived from mouse brains, including a reference to the corresponding idat files, in which the raw data are stored.

The microarray data discussed in this publication have been deposited in NCBI's Gene Expression Omnibus (Edgar et al., 2002) and are accessible through GEO Series accession number GSE119756 (https://www.ncbi.nlm.nih.gov/geo/query/acc.cgi?acc= GSE119756).

Figure 1

Fig. 1

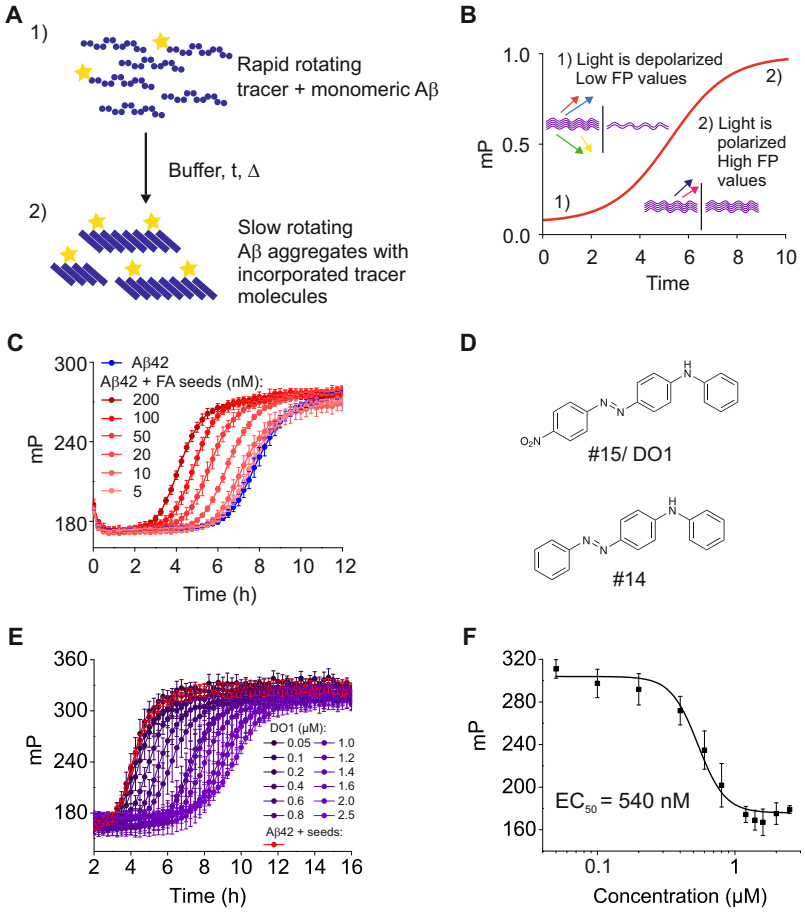

Figure 2

Fig. 2

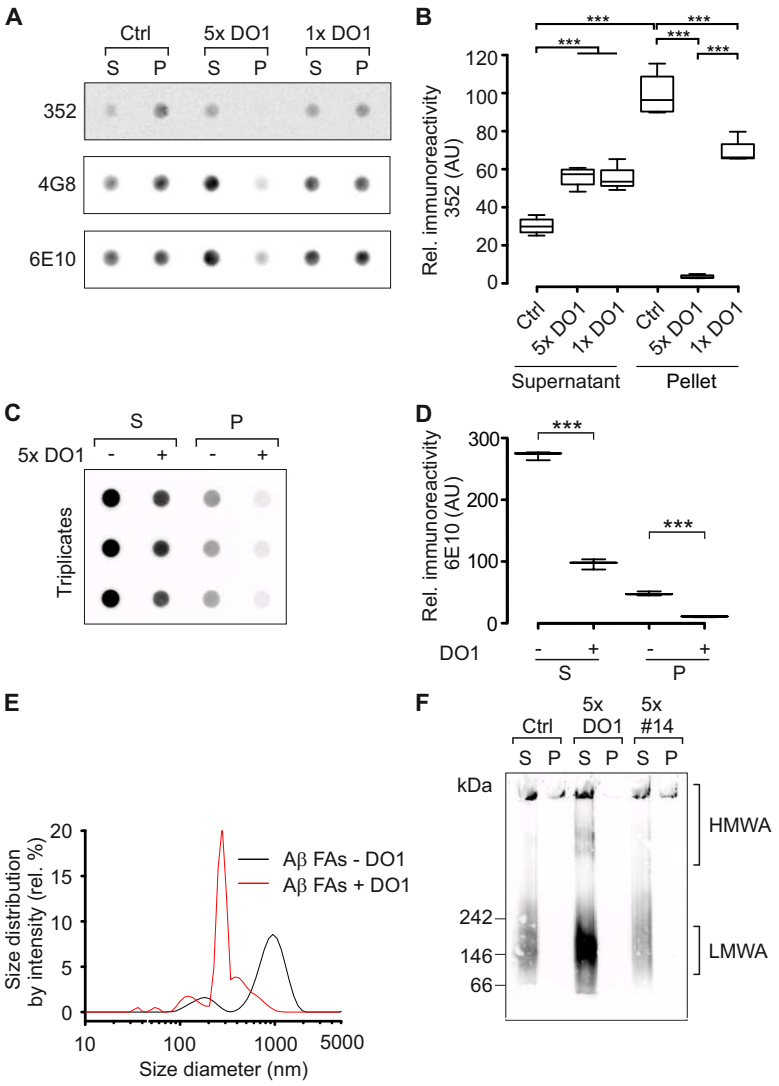

Figure 3

Fig. 3

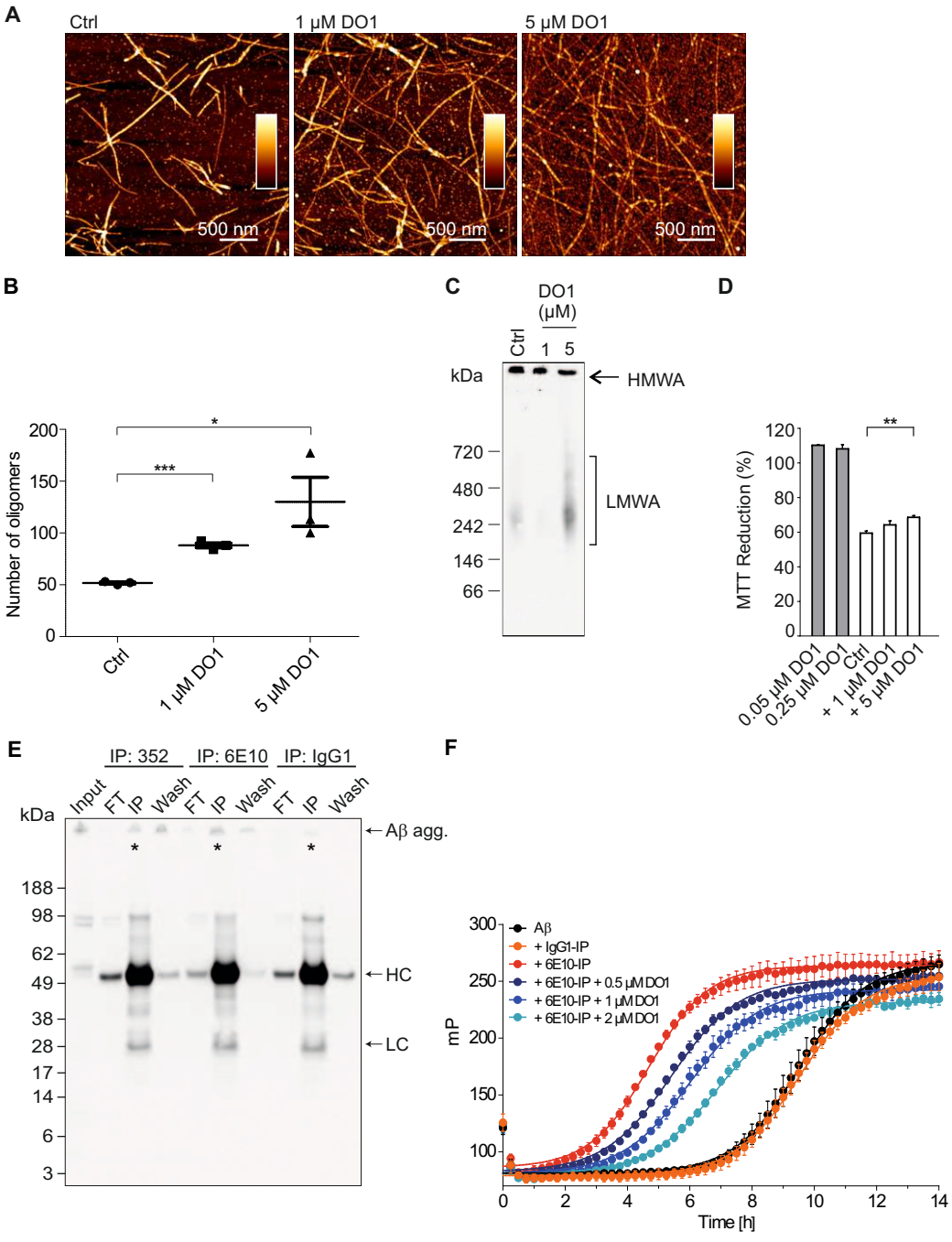

Figure 4

Fig. 4

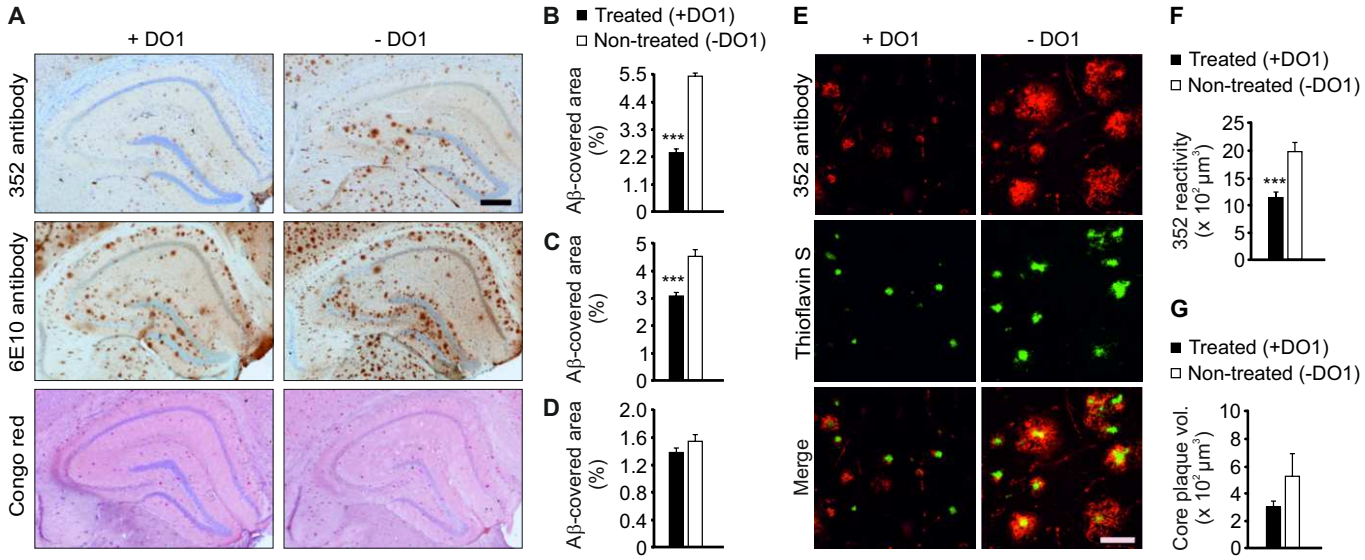

Figure 5

Fig. 5

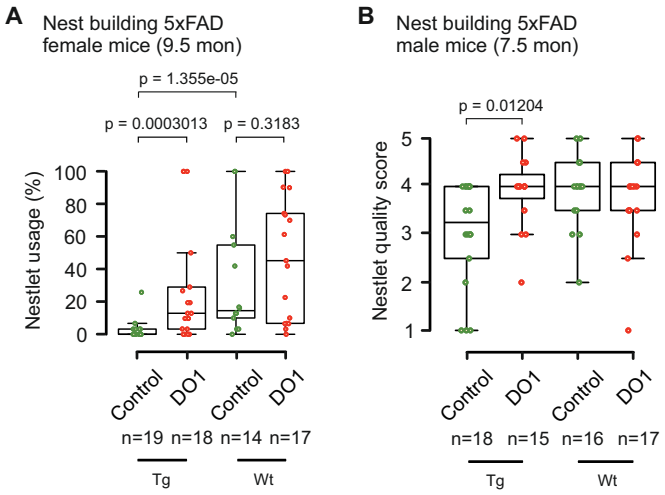

Figure 6

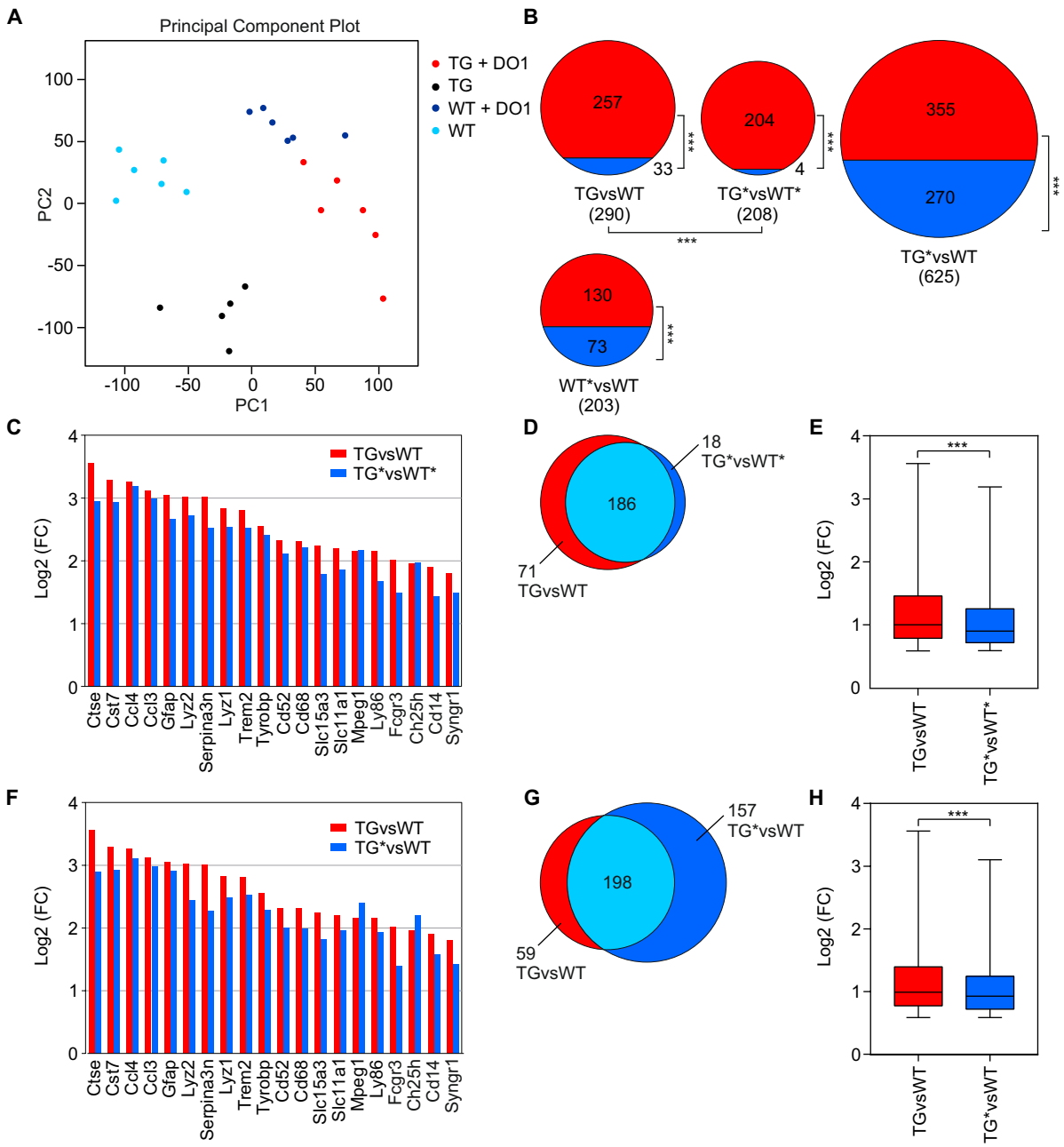
Fig.6
A
Principal Component Plot
TG + DO1
TG
WT + DO1
WT
PC1
PC2
B
257
33
TGvsWT
(290)
204
4
TG*vsWT*
(208)
355
270
TG*vsWT
(625)
130
73
WT*vsWT
(203)
***
C
TGvsWT
TG*vsWT*
Log2 (FC)
Ctse
Cst7
Ccl4
Ccl3
Gfap
Lyz2
Serpina3n
Lyz1
Trem2
Tyrobp
Cd52
Cd68
Slc15a3
Slc11a1
Mpeg1
Ly86
Fcgr3
Ch25h
Cd14
Syngr1
D
186
18
TG*vsWT*
71
TGvsWT
E
Log2 (FC)
TGvsWT
TG*vsWT*
F
TGvsWT
TG*vsWT
Log2 (FC)
G
198
157
TG*vsWT
59
TGvsWT
H
Log2 (FC)
TGvsWT
TG*vsWT

KEY RESOURCES TABLE

REAGENT or RESOURCE	SOURCE	IDENTIFIER
Antibodies		
antibody 352	This study	N/A
6E10	Biolegend	Cat#803017, RRID: AB_2565327
4G8	Biolegend	Cat#800711, RRID: AB_2565324
anti-amyloid fibrils OC antibody	Merck Millipore	Cat#AB2286, RRID: AB_1977024
IgG1	ThermoFisher Scientific	Cat#02-6100, RRID: AB_2532935
anti-mouse IgG, peroxidase conjugated	Sigma	Cat#A0168, RRID: AB_257867
mouse monoclonal GFAP antibody	Synaptic Systems	Cat#173011, RRID: AB_2232308
rabbit polyclonal GFAP antibody	Synaptic Systems	Cat#173002, RRID: AB_887720
goat anti-mouse IgG	Jackson Immuno Research Laboratories	Cat#115-005-062, RRID: AB_2338452
peroxidase AffiniPure goat anti-rabbit IgG	Jackson Immuno Research Laboratories	Cat#111-035-144, RRID: AB_2307391
Alexa Fluor 488 goat anti-mouse IgG	Invitrogen	Cat#R37120, RRID: AB_2556548
peroxidase conjugated goat anti-mouse IgG	Jackson Immuno Research Laboratories	Cat#115-035-146, RRID: AB_2307392
Chemicals, Peptides		
amyloid-β (1-42) peptide	Dr. Volkmar-Engert, Charité, Berlin	custom synthesis
amyloid-β (1-42) peptide	Bachem	Cat#H-1368
GFAP protein	Synaptic Systems	Cat#173-OP
5-Carboxyfluorescein labeled β-amyloid (1-42) peptide	Anaspec	Cat#AS-23525-05
1,1,1,3,3,3-Hexafluoro-2-propanol	Sigma-Aldrich	Cat#105228
Thioflavin T	Sigma-Aldrich	Cat#T3516
Pittsburgh Compound B	Chiroblock GmbH	custom synthesis
Sudan Orange G	Riedel-de-Haën	Cat#32670
RO 90-7501	Sigma-Aldrich	Cat#R0529
Butter Yellow	Fluka	Cat#73225
RS-0406	Chiroblock GmbH	custom synthesis
Methylene Blue	Fluka	Cat#66720
scyllo-Inositol	Sigma-Aldrich	Cat#I8132
Tramiprosate	Acros Organics	Cat#104430010
Azobenzene	Acros Organics	Cat#401540050
Orange GS	Aldrich	Cat#S472646
Disperse Orange 3	Acros Organics	Cat#201620500
Disperse Red 1	Aldrich	Cat#344206
4-(Phenylazo)diphenylamine	Acros Organics	Cat#21210250

Disperse Orange 1 (DO1)	Acros Organics	Cat#199410500
Congo red	Sigma-Aldrich	Cat#C6277
Biological Samples		
APPPS1 mouse brain	Dr. Frank Heppner (Charité, Berlin)	N/A
5xFAD mouse brain	This paper	N/A
Critical Commercial Assays		
nitrocellulose membrane, 0.1 µm (Dot blot assay)	GE Healthcare	Cat#10600000
nitrocellulose membrane, 0.45 µm (Western blot)	GE Healthcare	Cat#10600002
cellulose acetate membrane, 0.2 µM (Native filter retardation assay)	GE Healthcare	Cat#10404180
NativePAGE Novex 4-16% Bis-Tris gel	ThermoFisher Scientific	Cat#BN1004BOX
NuPAGE Novex 4-12% Bis-Tris	ThermoFisher Scientific	Cat#NP0323BOX
Mica	Plano	Cat#G-250-2
CellTiter 96® Non-Radioactive Cell Proliferation Assay (MTT)	Promega	Cat#G4000
ChemiGlow	Biozym	Cat#541015
Illumina™ TotalPrep™ RNA Amplification Kit	ThermoFisher Scientific	Cat#AMIL1791
Deposited data		
Raw and analysed microarray data	This paper	GEO: GSE119756 (https://www.ncbi.nlm.nih.gov/geo/query/acc.cgi?acc= GSE119756)
Experimental Models: Organisms/Strains		
5xFAD mice	The Jackson Laboratory	MMRRC Stock No: 34840-JAX, RRID: MMRRC-034840-JAX
BL6SJLF1/J mice	The Jackson Laboratory	Stock No: 100012, RRID: IMSR_JAX:100012
Software and Algorithms		
R version 3.4.0	R Development Core Team, 2006	https://www.r-project.org/
Beadarray (R package)	Dunning et al., 2007	https://bioconductor.org/packages/release/bioc/html/beadarray.html
ArrayQualityMetrics (R package)	Kauffmann et al., 2009	https://bioconductor.org/packages/release/bioc/html/arrayQualityMetrics.html
Limma (R package)	Ritchie et al., 2015	https://bioconductor.org/packages/release/bioc/html/limma.html
Ingenuity Pathway Analysis (IPA)	Kramer et al., 2014	https://www.qiagenbioinformatics.com/products/ingenuity-pathway-analysis/
Student's t-Test	CSBSJU Minnesota	http://www.physics.csbsju.edu/stats/t-test.html
Other		
Standard protocol for antibody production	Synaptic Systems	https://www.sysy.com/services/index.php

Fig. S1

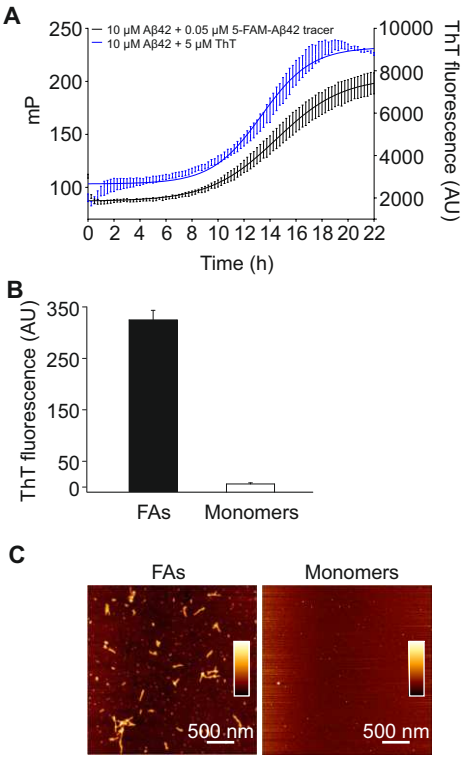
A
10 μM Aβ42 + 0.05 μM 5-FAM-Aβ42 tracer
10 μM Aβ42 + 5 μM ThT
mP
ThT fluorescence (AU)
Time (h)
B
ThT fluorescence (AU)
FAs
Monomers
C
FAs
Monomers
500 nm
500 nm

Fig. S2

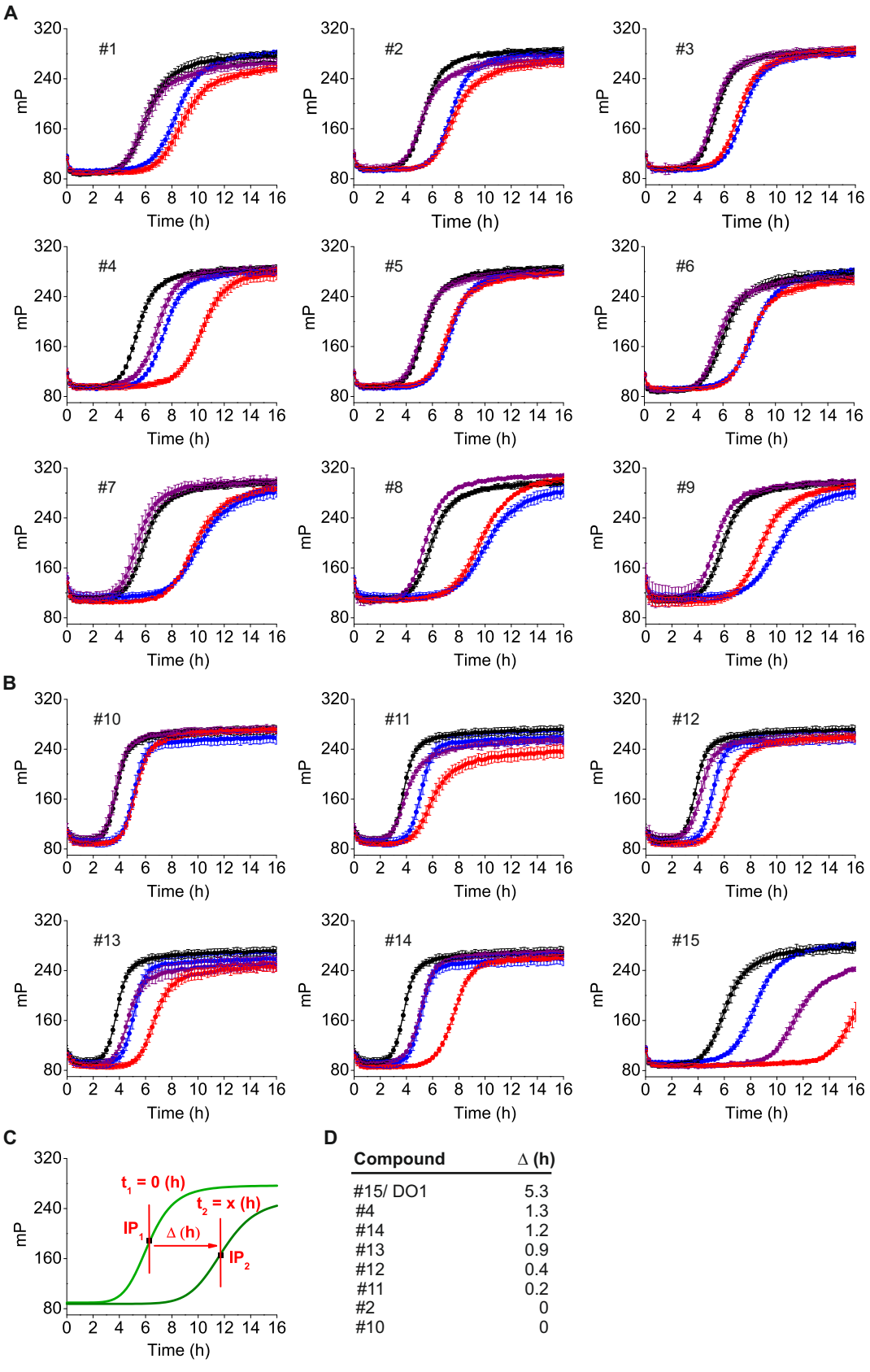

D

Compound	Δ (h)
#15/ DO1	5.3
#4	1.3
#14	1.2
#13	0.9
#12	0.4
#11	0.2
#2	0
#10	0

Fig. S3

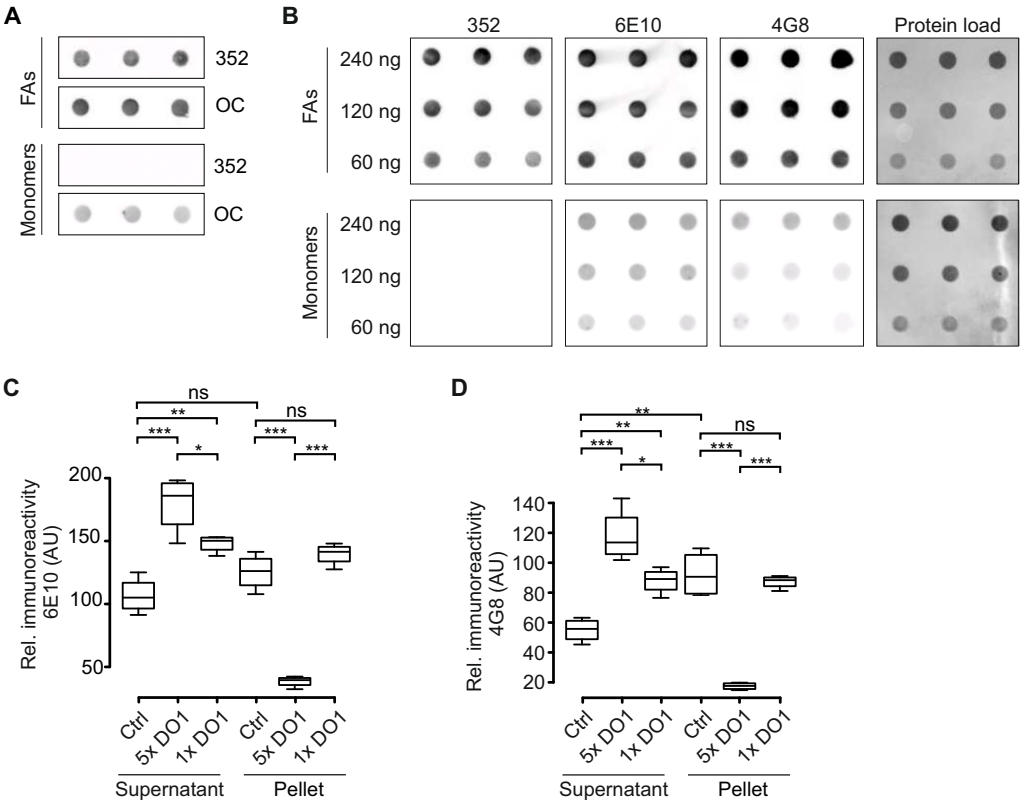
A
FAs
352
OC
Monomers
352
OC
B
352
6E10
4G8
Protein load
FAs
240 ng
120 ng
60 ng
Monomers
240 ng
120 ng
60 ng
C
Rel. immunoreactivity 6E10 (AU)
200
150
100
50
ns
**
***
*
ns
***
***
Ctrl
5x DO1
1x DO1
Ctrl
5x DO1
1x DO1
Supernatant
Pellet
D
Rel. immunoreactivity 4G8 (AU)
140
120
100
80
60
40
20
**
**
***
*
ns
***
***
Ctrl
5x DO1
1x DO1
Ctrl
5x DO1
1x DO1
Supernatant
Pellet

Fig. S4

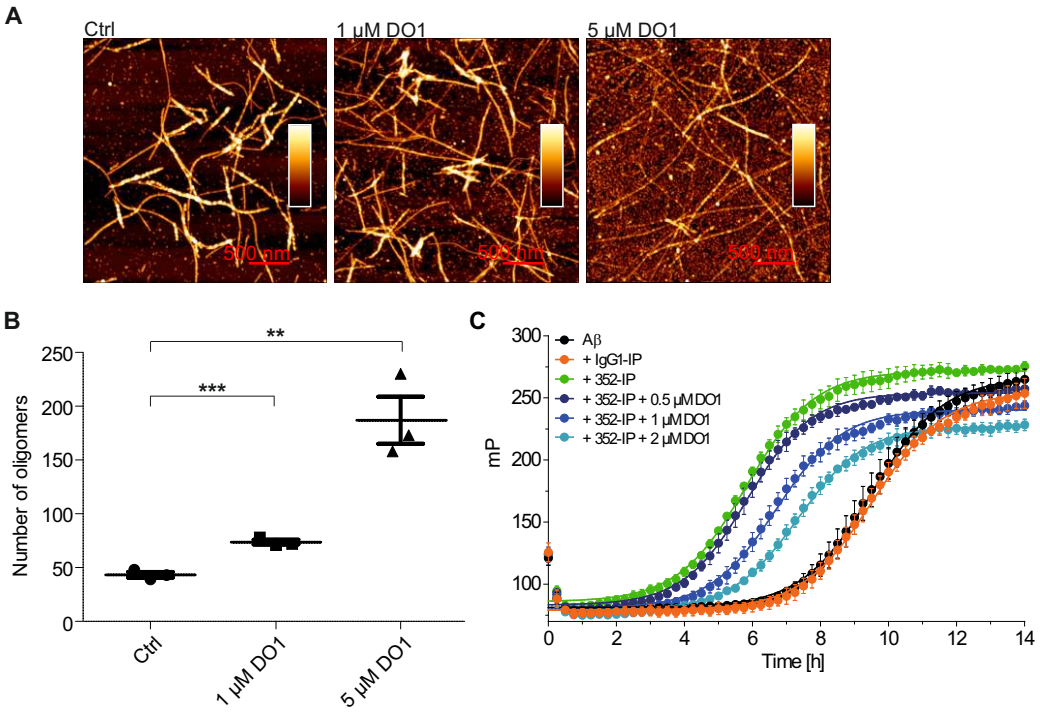
A
Ctrl
1 µM DO1
5 µM DO1
500 nm
500 nm
500 nm
B
Number of oligomers
250
200
150
100
50
0
**
***
Ctrl
1 µM DO1
5 µM DO1
C
mP
300
250
200
150
100
Aβ
+ IgG1-IP
+ 352-IP
+ 352-IP + 0.5 µM DO1
+ 352-IP + 1 µM DO1
+ 352-IP + 2 µM DO1
0
2
4
6
8
10
12
14
Time [h]

Fig. S5

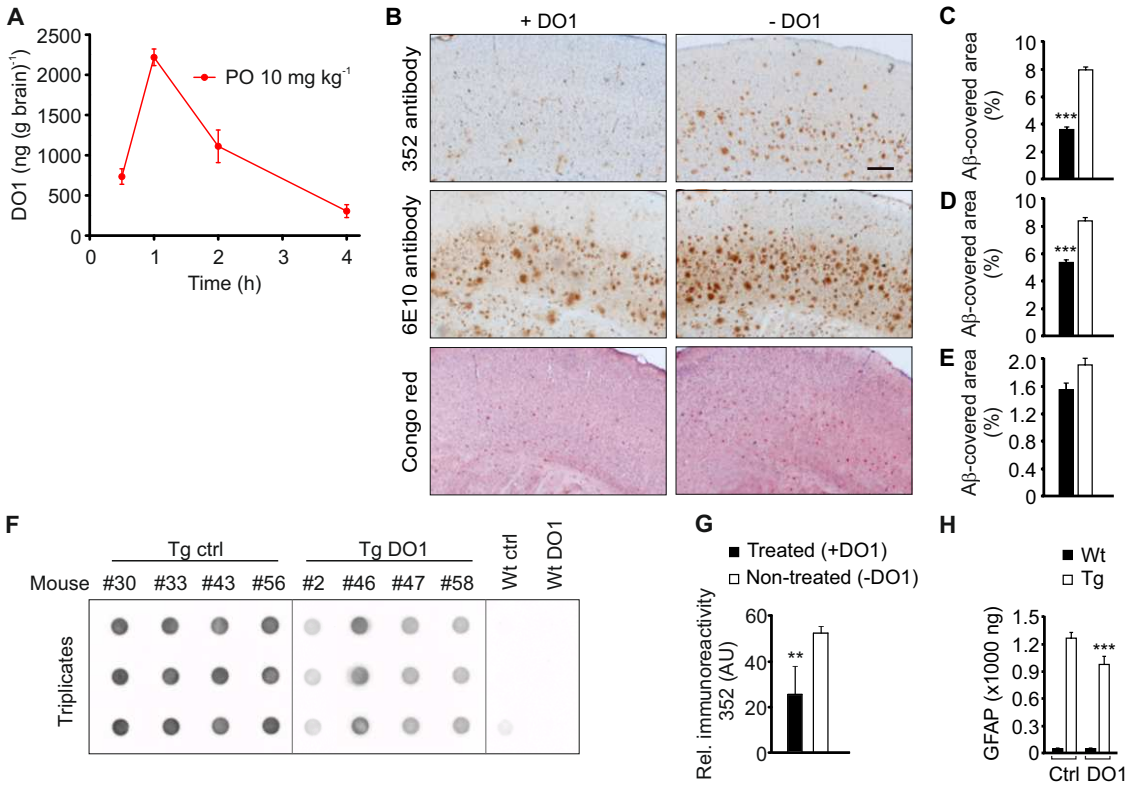
A
DO1 (ng (g brain)-1)
PO 10 mg kg-1
Time (h)
B
+ DO1
- DO1
352 antibody
6E10 antibody
Congo red
C
Aβ-covered area (%)
D
Aβ-covered area (%)
E
Aβ-covered area (%)
F
Tg ctrl
Tg DO1
Mouse #30 #33 #43 #56 #2 #46 #47 #58
Wt ctrl
Wt DO1
Triplicates
G
Treated (+DO1)
Non-treated (-DO1)
Rel. immunoreactivity 352 (AU)
H
Wt
Tg
GFAP (x1000 ng)
Ctrl DO1

Fig. S6

A TGvsWT

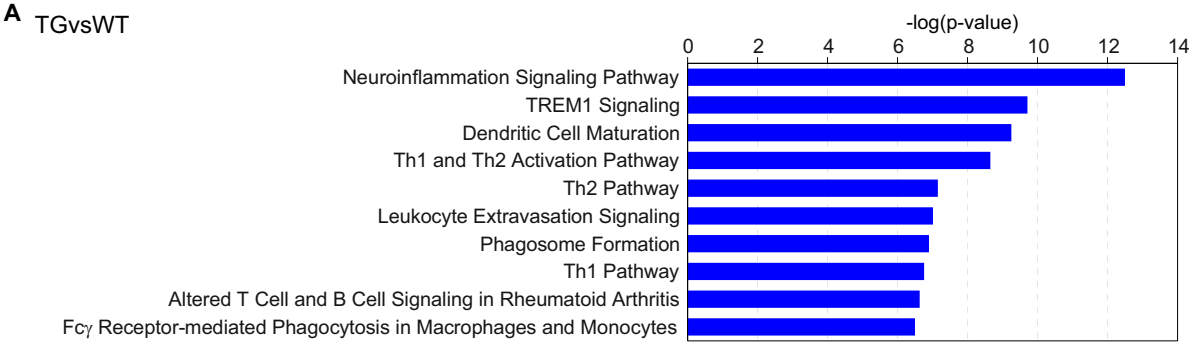

B TG*vsWT*

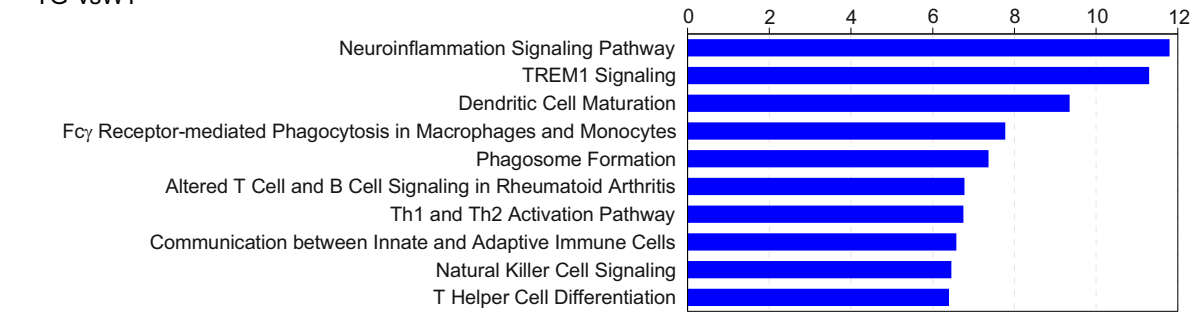

C TG*vsWT

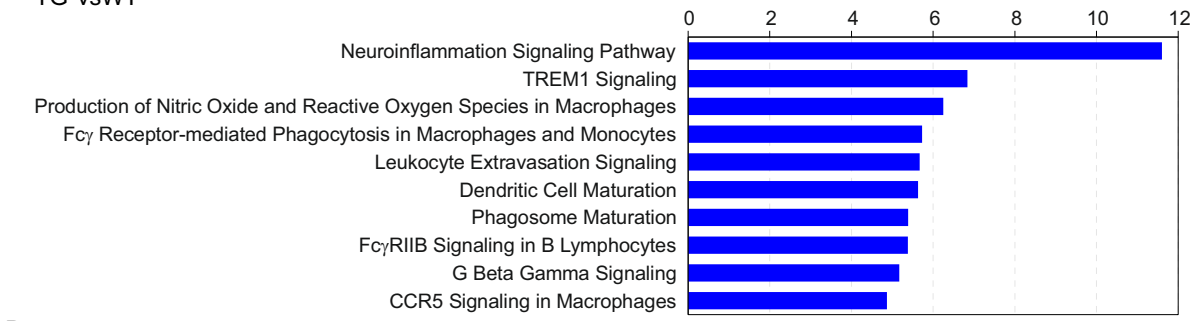

D WT*vsWT

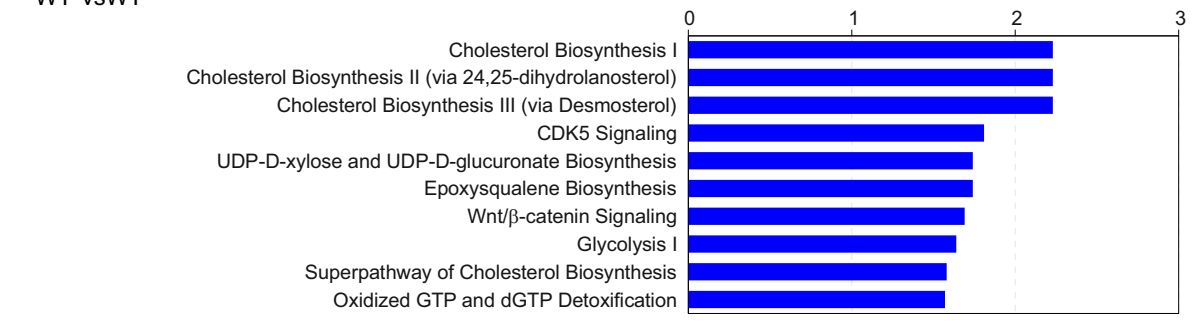

Figure S1 (related to Figure 1). Biochemical characterization of preformed Aβ42 seeds.

(**A**) Thioflavin T (ThT) fluorescence (arbitrary units, AU) and fluorescence polarization (milli-polarization, mP) were measured over time in spontaneous polymerization reactions. ThT and FP values were recorded at 440/485 and 470/528 nm, respectively. ThT and FP assays were performed in quadruplicates. The results of one experiment are shown (mean ± SD). (**B**) ThT fluorescence measurement of preformed Aβ42 fibrillar aggregates (FAs; 4.5 μM monomer equivalents) and monomers (4.5 μM) measured in arbitrary units (AU). Data represent mean ± SD. Average values were derived from triplicates of each sample. (**C**) Analysis of preformed Aβ42 FAs and monomers by atomic force microscopy using FESP silicon probes. Color gradient: 0-20 nm height.

Figure S2 (related to Figure 1). Analysis of compound effects on seeded and non-seeded ^{FAM}Aβ42/ Aβ42 co-aggregation with FP assays.

(**A**) Effects of potential aggregation modulators from the literature (#1 - #9, 1 μM) on seeded and non-seeded ^{FAM}Aβ42/Aβ42 co-polymerization (10 μM; black: Aβ42 with seeds; blue: Aβ42 w/o seeds; violet: Aβ42 with seeds and compound; red: Aβ42 with compound and w/o seeds). (**B**) Effects of azo compounds #10 - #15 (1 μM) on seeded and non-seeded ^{FAM}Aβ42/Aβ42 co-aggregation reactions (10 μM; black: Aβ42 with seeds; blue: Aβ42 w/o seeds; violet: Aβ42 with seeds and compound; red: Aβ42 with compound and w/o seeds). (**C**) Quantification of the inhibitory effect of compounds on seeded ^{FAM}Aβ42/Aβ42 co-aggregation. The inflection point (IP_1) of the seeded but untreated aggregation curve was set at zero; the time shift of the corresponding inflection point (IP_2) of the compound-treated seeded aggregation reactions was

expressed as Δ-value in hours. (**D**) Summary of the inhibitory effects of the tested compounds #2, #4, #10 - #14 and #15/ DO1 on seeded Aβ42 aggregation expressed as shift of the inflection points. Data in ***A*** and ***B*** represent mean ± SD.

Figure S3 (related to Figure 2). Analysis of Aβ42 fibrillar assembles (FAs) and monomers in DBAs using the antibodies 352, 6E10, 4G8 and OC.

DBAs revealed that the monoclonal antibody 352 detects preformed Aβ42 FAs but not monomers. In comparison, both FAs and monomers were recognized by the antibodies OC (**A**), 6E10 and 4G8 (**B**). Staining of membranes with amido black confirmed that similar amounts of Aβ42 monomers and FAs were analyzed. In (**A**) 120 ng of FAs and monomers were immobilized on membrane. (**C, D**) Box plot quantification of DBAs shown in Figure 2A, main text. **(C)** Quantification of 6E10 and (**D**) of 4G8 immunoreactivities. Two-way analysis of ANOVA showed a significant DO1 treatment effect ($F(2,18) = 15.39$, $p = 0.000127$) and position (antibody reactivity in pellet versus supernatant) effect ($F(1,18) = 64.88$, $p = 2.22e\text{-}07$) for 6E10 DBAs. There was also a significant interaction between treatment and position effects ($F(2,18) = 83.41$, $p = 7.88e\text{-}10$). For 4G8, the two-way ANOVA analysis revealed a treatment effect of $F(2,18) = 6.97$, $p=0.00573$; a position effect of $F(1,18) = 22.85$, $p = 0.00015$; and an interaction between treatment and position effects $F(2,18) = 84.90$, $p = 6.83e\text{-}10$.

Figure S4 (related to Figure 3). Effects of DO1 on seed-mediated amyloid assembly.

(A) AFM analysis of aggregate species derived from seed-mediated FAM-Aβ42 (0.05 µM)/Aβ42 (10 µM) co-aggregation reactions after incubation of samples for 18h. Color gradient: 0-10 nm height, except for the sample with 5 µM DO1 where the height is 0-8 nm. Samples were analyzed using the AFM probe PPP-NCHAuD. (**B**) Quantification

of oligomers in seeded Aβ42 aggregation reactions shown in ***A***. Oligomers were counted in three different areas (0.5 x 0.5 µm each) of the respective AFM pictures shown in ***A***. Data show mean ± SEM. *** p<0.001, ** p<0.01, one-way ANOVA. (**C**) Effects of different concentrations of DO1 on the seeding activity of Aβ species immunoprecipitated from APPPS1 mouse brain homogenates using the 352 anti-Aβ antibody (352-IP; see Figure 3E main text). As a control IgG1 immunoprecipitates (IgG1-IP) were tested that show no seeding activity. Average values were derived from quadruplicates of each sample in the experiment. Data represent mean ± SD.

Figure S5 (related to Figure 4). Effects of DO1 on Aβ aggregation and GFAP levels in brains of AD transgenic mice.

(**A**) Assessment of the DO1 concentration in mouse brains. The DO1 concentration was determined after a single administration by oral gavage. 10 mg DO1 per kg mouse weight were applied; mouse brain extracts were analyzed by LC-MS. Per time point three male mice were used. Data represent mean ± SD. (**B-E**) Effects of DO1 treatment on Aβ plaque load in cortex of 5xFAD transgenic mice. (**B**) Immunohistochemical detection of Aβ plaques in the cortex of 5xFAD female mice treated for 8 months with 0.652 g DO1 per kg of mouse chow. Top and middle rows, 3,3'-diaminobenzidine (DAB) staining of Aβ plaques with 352 and 6E10 antibodies. Bottom rows, Congo red staining of dense core regions in Aβ plaques. DO1 treatment of 5xFAD mice significantly reduced 352 (**C**) and 6E10 (**D**) immunoreactivities (***p < 0.001 versus control, one-way ANOVA, n = 4-5 mice per group). (**E**) Quantification of Congo red stained dense core plaque regions of compound treated and untreated animals. Scale bar in ***B*** = 50 µm and applies to all images. Data represent mean ± SEM. (**F-H**) DO1 treatment decreases the abundance of Aβ aggregates and reduces GFAP levels in brains of AD transgenic mice. (**F**) Analysis of 352-reactive Aβ aggregates in brain

homogenates, prepared from hemispheres of 7.5 month-old DO1 treated and untreated (ctrl) male 5xFAD transgenic (Tg) mice by native filter retardation assays (FRAs). Brain homogenates of wild-type (Wt) DO1 treated and untreated mice were analyzed as control. Similarly, we assessed homogenates of treated and untreated AD transgenic mice. (**G**) Quantification of results shown in ***F***. Data represent mean ± SD (**p < 0.01, unpaired two tailed t-test). (**H**) Analysis of GFAP protein levels in brain homogenates, prepared from hemispheres of 9.5 month-old DO1-treated and untreated 5xFAD female transgenic (Tg) and wild-type (Wt) mice (Wt ctrl n = 5, Tg ctrl n = 6, Wt DO1 n = 9, Tg DO1 n = 10) by ELISA (***p < 0.001, one-way ANOVA). Data represent mean ± SEM.

Figure S6 (related to Figure 6). IPA pathway analysis.

Presented are the top ten significantly (p < 0.05) dysregulated pathways obtained with the datasets: (**A)** TGvsWT, (**B)** TG*vsWT*, (**C)** TG*vsWT and **(D)** WT*vsWT.

Table S1 (related to Figures 1 and 2)

No.	Trivial name/ Code (IUPAC Nomenclature)	Structure
#1	**Pittsburgh Compound B** (2-(4-(Methylamino)phenyl)benzo[*d*]thiazol-6-ol)	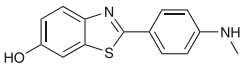
#2	**Sudan Orange G** (4-(Phenyldiazenyl)benzene-1,3-diol)	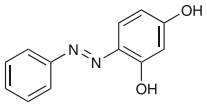
#3	**RO 90-7501** (2'-(4-aminophenyl)-1*H*,1'*H*-2,5'-bibenzo[*d*]imidazol-5-amine)	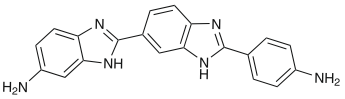
#4	**Butter Yellow** (*N*,*N*-Dimethyl-4-(phenyldiazenyl)aniline)	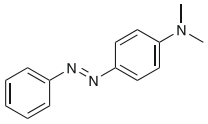
#5	**RS-0406** (3,3'-(Pyridazine-3,6-diylbis(azanediyl))diphenol)	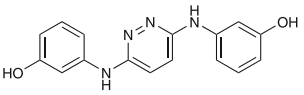
#6	**Methylene Blue** (*N*-(7-(Dimethylamino)-3*H*-phenothiazin-3-ylidene)-*N*-methylmethanaminium chloride)	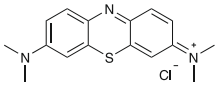
#7	**scyllo-Inositol** ((1r,2r,3r,4r,5r,6r)-cyclohexane-1,2,3,4,5,6-hexaol)	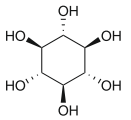
#8	**Thioflavin T** (2-(4-(Dimethylamino)phenyl)-3,5-dimethylbenzo[*d*]thiazol-3-ium chloride)	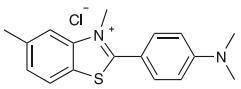
#9	**Tramiprosate** (3-Aminopropane-1-sulfonic acid)	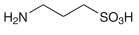
#10	**Azobenzene** (1,2-Diphenyldiazene)	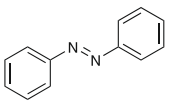
#11	**Orange GS** (Sodium 4-((4-(phenylamino)phenyl)diazenyl)benzenesulfonate)	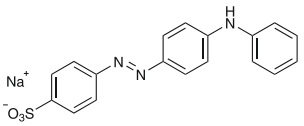
#12	**Disperse Orange 3** (4-((4-Nitrophenyl)diazenyl)aniline)	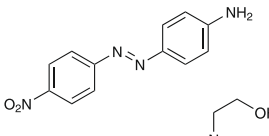
#13	**Disperse Red 1** (2-(Ethyl(4-((4-nitrophenyl)diazenyl)phenyl)amino)ethanol)	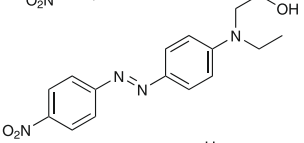
#14	**4-(Phenylazo)diphenylamine** (*N*-Phenyl-4-(phenyldiazenyl)aniline)	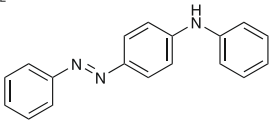
#15	**Disperse Orange 1 (DO1)** (4-((4-Nitrophenyl)diazenyl)-*N*-phenylaniline)	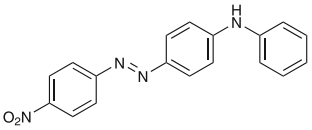

Table S1 (related to Figures 1 and 2). Overview of tested chemical compounds using the FP assay.

The list of small molecules contains known amyloid aggregate binders as well as compounds that have not previously been shown to interact with amyloid structures.